NeuroImage 201 (2019) 115985

Contents lists available at ScienceDirect

NeuroImage

journal homepage: www.elsevier.com/locate/neuroimage

Thalamic low frequency activity facilitates resting-state cortical interhemispheric MRI functional connectivity

Xunda Wang [a,b,1], Alex T.L. Leong [a,b,1], Russell W. Chan [a,b,c], Yilong Liu [a,b], Ed X. Wu [a,b,*]

[a] Laboratory of Biomedical Imaging and Signal Processing, The University of Hong Kong, Hong Kong, China
[b] Department of Electrical and Electronic Engineering, The University of Hong Kong, Hong Kong, China
[c] Department of Neurology and Neurological Sciences, Stanford University, Stanford, United States

ARTICLE INFO

Keywords:
Resting-state MRI functional connectivity
Thalamus
Optogenetic
fMRI
Cortical layers

ABSTRACT

Blood-oxygen-level-dependent (BOLD) resting-state functional MRI (rsfMRI) has emerged as a valuable tool to map complex brain-wide functional networks, predict cognitive performance and identify biomarkers for neurological diseases. However, interpreting these findings poses challenges, as the neural basis of rsfMRI connectivity remains poorly understood. The thalamus serves as a relay station and modulates diverse long-range cortical functional integrations, yet few studies directly interrogate its role in brain-wide rsfMRI connectivity. Utilizing a multi-modal approach of rsfMRI, optogenetic stimulation and multi-depth cortical electrophysiology recording, we examined whether and how the somatosensory thalamus contributes to cortical interhemispheric rsfMRI connectivity. We found that low frequency (1 Hz) optogenetic stimulation of somatosensory-specific ventral posteromedial (VPM) thalamocortical excitatory neurons increased the interhemispheric rsfMRI connectivity in all examined sensory cortices, somatosensory, visual and auditory, and the local intrahemispheric BOLD activity at infraslow frequency (0.01–0.1 Hz). In parallel, multi-depth local field potential recordings at bilateral primary somatosensory cortices revealed increased interhemispheric correlations of low frequency neural oscillations (i.e., mainly < 10 Hz) at all cortical layers. Meanwhile, pharmacologically inhibiting VPM thalamocortical neurons decreased interhemispheric rsfMRI connectivity and local intrahemispheric infraslow BOLD activity in all sensory cortices. Taken together, our findings demonstrate that low frequency activities in the thalamo-cortical network contribute to brain-wide rsfMRI connectivity, highlighting the thalamus as a pivotal region that underlies rsfMRI connectivity.

1. Introduction

The brain consists of numerous interconnected parallel and hierarchical networks subserving sensory, behavioral and cognitive functions (Park and Friston, 2013). Resting-state functional MRI (rsfMRI) enables non-invasive visualization of long-range brain-wide functional connectivity networks between anatomically separated, but functionally related, brain regions during rest based on coherent spontaneous blood-oxygen-level-dependent (BOLD) activity (Biswal et al., 1995; Chan et al., 2017; Fox and Raichle, 2007; Smith et al., 2013). A fast-growing body of literature utilizes rsfMRI connectivity as a robust tool to study complex brain-wide functional networks. In recent years, these intrinsic rsfMRI connectivity networks and their changes in normal and diseased brains have emerged in the scientific and clinical community as important biomarkers to predict cognitive performance and disease state (Chuang and Nasrallah, 2017; Cole et al., 2016; Drysdale et al., 2017; Miller et al., 2016; Shen et al., 2018). Since cortical interhemispheric rsfMRI connectivity can be detected robustly across species, it has gained

Abbreviations: MRI, functional magnetic resonance imaging; rsfMRI, Resting-state functional MRI; BOLD, blood-oxygen-level-dependent; VPM, ventral posteromedial; S1BF, somatosensory barrel field; S2, secondary somatosensory cortex; V1, primary visual cortex; A1, primary auditory cortex; LFP, local field potential; CSD, current source density; TTX, tetrodotoxin; CULATR, Committee on the Use of Live Animals in Teaching and Research; AAV, Adeno-associated virus; OG, optogenetic; RARE, Rapid Acquisition with Refocused Echoes; T2W, T2-weighted; FOV, field of view; TE, echo time; TR, repetition time; GE-EPI, gradient-echo echo-planar-imaging; SBA, seed-based analysis; ROI, region of interest; CC, correlation coefficient; FWHM, full width at half maximum; PFA, para-formaldehyde; PBS, phosphate buffered saline.

* Corresponding author. Laboratory of Biomedical Imaging and Signal Processing, Department of Electrical and Electronic Engineering, School of Biomedical Sciences, Department of Medicine, The University of Hong Kong, Pokfulam, Hong Kong, China.
E-mail address: ewu@eee.hku.hk (E.X. Wu).
[1] Authors contributed equally to this work.

https://doi.org/10.1016/j.neuroimage.2019.06.063
Received 14 December 2018; Received in revised form 18 June 2019; Accepted 26 June 2019
Available online 9 July 2019

prominence as a key model to explore the neural bases of rsfMRI connectivity. For example, several human and animal studies have reported preserved cortical interhemispheric rsfMRI connectivity in subjects with congenital agenesis (Tovar-Moll et al., 2014; Tyszka et al., 2011) or partial damage (O'Reilly et al., 2013; Roland et al., 2017; Zhou et al., 2014) of the interhemispheric corpus callosum connections. In-depth interpretations of these rsfMRI findings are challenging, as little is explicitly known about the neural bases underlying rsfMRI connectivity. These observations do strongly suggest the involvement of subcortical regions and polysynaptic connections in maintaining and supporting brain-wide rsfMRI connectivity. However, the exact contributions of subcortical regions (e.g., thalamus) and polysynaptic connections to brain-wide rsfMRI connectivity are still poorly understood, primarily owing to the lack of studies directly interrogating their roles in brain-wide cortical rsfMRI connectivity.

Thalamus relays and modulates diverse long-range functional neural integrations involved in cortical processing (Hwang et al., 2017; Rikhye et al., 2018; Sherman, 2016). Meta-analyses of large task-based neuroimaging dataset indicated thalamic engagement in numerous cognitive functions (Crossley et al., 2013; Hwang et al., 2017). Electrophysiology studies revealed that the thalamus can control cortical states and modulate the flow of information processing during cognitive processes (Alonso and Swadlow, 2015; Nakajima and Halassa, 2017; Poulet et al., 2012; Sherman, 2016). Unfortunately, previous attempts to infer thalamic contributions to brain-wide rsfMRI connectivity using graph theory-based analyses have generated inconclusive results. Some studies found that the thalamus is a critical region to promote global communication and information integration in brain-wide rsfMRI connectivity (Cole et al., 2010; Crossley et al., 2013; Hwang et al., 2017), while several other found the opposite (X. Liang et al., 2018; Power et al., 2013; van den Heuvel and Sporns, 2013; Zalesky et al., 2014). To determine whether and how the thalamus contributes to brain-wide rsfMRI connectivity, it is imperative to directly perturb thalamus and monitor the rsfMRI connectivity with a multi-modal approach of rsfMRI, neuromodulation (e.g., optogenetics) and electrophysiology recordings.

Polysynaptic connections may underlie and maintain brain-wide rsfMRI connectivity, especially cortical interhemispheric rsfMRI connectivity (O'Reilly et al., 2013; Roland et al., 2017; Tovar-Moll et al., 2014; Tyszka et al., 2011; Zhou et al., 2014). The cerebral cortex contains an intricate laminar and columnar architecture, which has extensive polysynaptic connections within itself and with the thalamus to form brain-wide thalamo-cortical networks (Sherman, 2017). Such properties enable diverse long-range functional neural interactions. For example, somatosensory cortical neurons first receive somatosensory thalamic inputs at layer IV and V before transmission to other cortical neurons across multiple layers and columns in somatosensory cortices (Douglas and Martin, 2004; Feldmeyer, 2012; Thomson and Bannister, 2003) and other sensory cortices (M. Liang et al., 2013), before returning to the thalamus (Sherman, 2016, 2017). Hence, neural activity initiated in the thalamus could recruit multiple cortical regions via cortico-cortical pathway, which consists of interhemispheric corpus callosum, cross-modal, and cortico-thalamo-cortical connections that involve multiple cortical layers (Douglas and Martin, 2004; Leong et al., 2016; Sherman, 2016; Thomson and Bannister, 2003; Zingg et al., 2014). Meanwhile, all thalamic nuclei are also connected to the thalamic reticular nucleus within the same hemisphere (Halassa et al., 2014; Lam and Sherman, 2007, 2011; Lewis et al., 2015). Hence, thalamic nucleus could also activate multiple thalamic nuclei through this thalamo-thalamic pathway and subsequently influence multiple cortical regions without first directly recruiting multiple cortical layers across cortico-cortical connections. Thus, examining whether multiple cortical regions and layers are involved could help to elucidate the predominant polysynaptic pathway(s) recruited by the thalamus to mediate cortical interhemispheric rsfMRI connectivity. We will exploit this thalamo-cortical architecture and network as a model to study the contributions of subcortical inputs and polysynaptic connections to brain-wide rsfMRI connectivity.

Recent studies suggested low frequency (<10 Hz) spontaneous oscillatory neuronal activities as potential candidates to constrain and elicit rsfMRI BOLD activity, since these oscillations resemble spatiotemporal patterns of rsfMRI signals during anesthesia, sleep and awake states (Ma et al., 2016; Matsui et al., 2016; Pan et al., 2013; Schölvinck et al., 2010; Wang et al., 2012). Slow (0.5–1.5 Hz), delta (1.5–4 Hz) and spindle (7–14 Hz) oscillations have been identified as the unique characteristics in thalamo-cortical networks (Crunelli et al., 2015; Fernandez et al., 2017; Mak-McCully et al., 2017; Neske, 2015). Specifically, the thalamus participates in long-range brain-wide propagation of slow cortical activity (David et al., 2013; Stroh et al., 2013; Xiao et al., 2017) and brain-wide coupling of spontaneous oscillatory neural events (Dudai et al., 2015; Latchoumane et al., 2017; Staresina et al., 2015) through thalamo-cortical or thalamo-hippocampal-cortical networks. Our recent fMRI investigation directly demonstrated that low frequency (1 Hz) neural activity optogenetically initiated at somatosensory thalamus robustly propagates throughout the brain to bilateral sensory cortices (Leong et al., 2016). These studies highlight the pivotal roles the thalamus plays in propagating and synchronizing neural oscillations across the brain. They also indicate the thalamus is an ideal target to perturb for delineating the relationship between rsfMRI connectivity and neural oscillations.

Investigation of whether and how ascending sensory inputs influence cortical rsfMRI connectivity can provide in-depth understanding into how subcortical regions and polysynaptic connections contribute to brain-wide rsfMRI connectivity. There has been numerous research on revealing the relevance of rsfMRI connectivity networks to task activations (Cole et al., 2016; Smith et al., 2009; Tavor et al., 2016), and showing that either sensory stimulation or task performance can modulate intrinsic rsfMRI connectivity networks (Chuang and Nasrallah, 2017; Harmelech et al., 2013; J. Li et al., 2015; Nasrallah et al., 2016). However, such external task-based paradigms cannot identify the key sources or players (e.g., thalamic activities) in the ascending sensory pathways that contribute to brain-wide rsfMRI connectivity. An intuitive way to identify some of these sources is to examine the changes in rsfMRI functional connectivity by selectively modulating the thalamocortical neurons of sensory thalamic nuclei. Structural connections and characteristics of activity propagation between ventral posteromedial thalamus (VPM) and the cortical layers of primary somatosensory barrel field (S1BF) are well-studied in the rodent brain (Constantinople and Bruno, 2013; Cruikshank et al., 2010; Viaene et al., 2011a, 2011b). Furthermore, recent studies have demonstrated that the VPM can recruit brain-wide polysynaptic activity and modulate functions beyond the somatosensory system (Leong et al., 2016; Xiao et al., 2017), indicating the potentially important role of VPM in complex polysynaptic networks that support brain-wide cortical rsfMRI connectivity. Taken together, we chose VPM as a neuromodulation target to provide pivotal insights into the contributions of sensory thalamus to brain-wide rsfMRI connectivity.

Here, we examined whether and how the somatosensory thalamus influences cortical interhemispheric rsfMRI connectivity within and beyond the somatosensory modality. We directly perturbed the VPM and monitored brain-wide resting-state functional connectivity changes using rsfMRI and electrophysiology recordings at bilateral somatosensory cortices before and after low frequency (1 Hz) optogenetic stimulation of VPM thalamocortical excitatory neurons. We also examined whether pharmacological inhibition of VPM thalamocortical neurons would decrease cortical interhemispheric rsfMRI connectivity.

2. Materials and methods

2.1. Animal subjects, virus packaging and stereotactic surgery for viral injection

All animal experiments were approved by the University of Hong Kong's Committee on the Use of Live Animals in Teaching and Research

(CULATR). Three groups of age-matched adult male Sprague Dawley rats were used in this study (i.e., two groups comprising of optogenetically transfected animals and the other with naïve animals). Two of these animal groups underwent rsfMRI experiments (optogenetic: n = 8; tetrodotoxin, TTX: n = 10), whereas the other underwent local field potential (LFP) recording experiments (optogenetic: n = 9).

Recombinant Adeno-associated virus (AAV) vectors were serotyped with AAV5 coat proteins and produced by the vector core at the University of North Carolina at Chapel Hill, Chapel Hill, NC. Viral titer (in particles per milliliter) was 4×10^{12} for AAV5-CaMKIIα-ChR2(H134R)-mCherry. Maps are available online from www.stanford.edu/group/dlab/optogenetics.

All stereotactic surgeries for viral injection were performed with rats at 6–7 weeks of age. Rats were anesthetized with an intraperitoneal bolus injection of a ketamine (90 mg/kg) and xylazine (40 mg/kg) mixture. Following a small craniotomy, viral injections were performed at two depths in VPM (−3.6 mm posterior to Bregma, +3.0 mm medial-lateral right hemisphere, −5.8 and −6.2 mm from the surface of dura). Three microliters of viral constructs (1.5 μL at each depth) were delivered through a 5-μL syringe and 33-gauge beveled needle and injected at 150 nL/min. The injection needle was held in place for 10 min before being slowly retracted from the brain. Scalp incision was sutured, and animals were kept on a heating pad until recovery from anesthesia. Buprenorphine (0.05 mg/kg, subcutaneous) was administered post-injection twice daily for 72 h to minimize discomfort. Enrofloxacin was also administered orally for 72 h to minimize infection and inflammation post-surgery. Animals recovered for 6–7 weeks before conducting MRI and electrophysiological experiments.

2.2. Animal preparation for optogenetic rsfMRI experiments and TTX rsfMRI experiments

Surgery was performed under 2% isoflurane to implant an opaque custom-made plastic optical fiber cannula (d = 450 μm) or a glass capillary tube (d = 300 μm) at VPM with high-resolution anatomical MRI verification. Note that the fiber cannula was made opaque using heat shrinkable sleeves to prevent light leakage during stimulation to elicit undesired visual stimulation. The fiber tip surface was beveled to facilitate the fiber insertion and minimize injury to brain tissue. Dental cement was applied to fix the fiber cannula or the glass capillary tube on the skull. The optical fiber tip was typically situated in the center of the VPM nucleus through stereotaxic implantation and verified by high-resolution anatomical MRI. The spatial spread from the fiber tip for 473 nm blue light is rather small (200 μm and 350 μm at 50% and 10% of initial light intensity, respectively) and has little or no spreading in the backward and lateral directions (Yizhar et al., 2011), confining the optogenetic stimulation within the VPM nucleus. Buprenorphine (0.05 mg/kg, subcutaneous) was administered subcutaneously post-implantation and one drop of 2% lidocaine was applied to the chords to minimize discomfort before endotracheal intubation and MRI experiments. The animals were mechanically ventilated at a rate of 60 breaths per minute with 1–1.5% isoflurane in room-temperature air using a ventilator (TOPO, Kent Scientific, Torrington, CT). During all fMRI experiments, animals were placed on a plastic holder, and their heads were fixed with a tooth bar and ear bars. Continuous physiological monitoring was performed using sensors of an MRI-compatible system (SA Instruments, Stony Brook, NY). Rectal temperature was maintained at ~37.0 °C using a water circulation system. Vital signs were within normal physiological ranges (rectal temperature: 36.5–37.5 °C, heart rate: 350–420 beat/min, breathing: ~60 breath/min and not synchronized to optogenetic stimulation, oxygen saturation: > 95%) throughout the duration of the experiments (Chan et al., 2017; Leong et al., 2016; Zhou et al., 2014).

2.3. MRI scanner-synchronized optogenetic stimulation and TTX infusion

For optogenetic rsfMRI experiments, an Arduino programming board synchronized the scanner trigger and the lasers for optogenetic stimulation. Computers and light delivery systems were kept outside the magnet and long optical patch cables (5–10 m) delivered light into the bore of the scanner. For optogenetic stimulation, blue light was delivered using a 473 nm Diode-pumped solid-state laser measured before scanning as 8 mW at the fiber-tip (450 μm, NA = 0.5) corresponding to a light intensity of 40 mW/mm^2. To examine the effects of low frequency (1 Hz) optogenetic stimulation of VPM on brain-wide rsfMRI connectivity, a total of thirteen sessions were acquired for each animal, three before (pre), five during (OG-On), and five after (post) optogenetic stimulation (Fig. 1). For each OG-On session, 1 Hz optogenetic stimulation (light intensity = 8 mW: 40 mW/mm^2; 5% duty cycle) was presented in a block design paradigm, which consists of two 2 min on 2 min off stimulation blocks (120 pulses; Fig. 1). Block design was used in favor of continuous optogenetic stimulation to minimize any unphysiological stimulation effects due to prolonged activation, while maintaining sufficient sensitivity in detecting rsfMRI connectivity changes. Note that random intervals were employed between each rsfMRI scan to minimize the entrainment effects on the neural activity caused by the regular periodic nature of the stimulation blocks. 1 Hz stimulation was employed mainly due to its efficiency in evoking long-range brain-wide low frequency activities (Leong et al., 2016), which we believe will give us the best chance to determine whether the perturbation of thalamus could influence brain-wide cortical interhemispheric rsfMRI connectivity.

For TTX rsfMRI experiments, a total of fifteen sessions were performed on each animal, five before (pre), and ten after (post) TTX infusion. The concentration of TTX used was 5 ng/μL, similar to the values used in our previous in vivo study (Chan et al., 2017).

2.4. MRI acquisition procedure

All MRI experiments were performed on a 7 T MRI scanner (PharmaScan 70/16, Bruker Biospin GmbH, Ettlingen, Germany) using a transmit-only birdcage coil in combination with an actively decoupled receive-only surface coil. A single channel receive-only surface coil was used for the optogenetic rsfMRI experiments and a three-channel receive-only surface coil with an opening for TTX rsfMRI experiments to accommodate the glass capillary tube used for TTX infusion. Despite the use of different coils, data acquired from the two groups at baseline (i.e., prior to optogenetic stimulation and TTX infusion, respectively) were comparable (Supplementary Fig. 1). After placing the animal in the magnet, scout and anatomical RARE T2-weighted (T2W) images were first acquired for accurate positioning and reference with field of view (FOV) = 32 × 32 mm^2, matrix = 256 × 256, RARE factor = 8, echo time (TE) = 36 ms, repetition time (TR) = 4200 ms. Sixteen contiguous 1.0-mm slices were positioned in the transverse orientation according to the rat brain atlas to cover the majority of the brain. All rsfMRI data were obtained at the same geometry as the anatomical reference T2W images, using a single-shot gradient-echo echo-planar imaging (GE-EPI) sequence with FOV = 32 × 32 mm^2, matrix = 64 × 64, flip angle = 50°, TE = 20 ms, TR = 750 ms. A total of 640 vol were collected during each session.

2.5. rsfMRI data analysis

rsfMRI preprocessing was performed using the standard procedure established in our previous studies (Chan et al., 2017; Leong et al., 2016; Zhou et al., 2014). For each rsfMRI session, all images were first corrected for slice timing differences and then realigned to the mean image of the first rsfMRI session using SPM12 (Wellcome Department of Imaging Neuroscience, University College London, UK). The T2W images from each animal were coregistered to a representative brain using affine transformation and Gaussian smoothing to maximize normalized mutual information (SPM12). The transformation matrix was then applied to coregister rsfMRI images. Voxel-wise linear detrending with least-squares estimation was subsequently performed temporally to

eliminate the baseline drift caused by physiological noises and system instability. This was then followed by applying a temporal band-pass filter (0.005–0.1 Hz) without spatial smoothing. Global signal regression was applied for removing non-neuronal global variance and facilitating the detection of interhemispheric rsfMRI connectivity (Birn, 2012; Fox et al., 2009; Murphy and Fox, 2017; Power et al., 2014; C.-G. Yan et al., 2013). Scans suffering from motion artifacts (>0.125 mm voxel shifts detected by realignment) and sudden physiological changes (i.e., abrupt changes in respiration pattern, heart rate and oxygen saturation level) were discarded.

To examine functional connectivity changes pre and post low frequency (1 Hz) optogenetic stimulation, seed-based analysis (SBA) was applied to map and quantify interhemispheric rsfMRI connectivity of primary somatosensory barrel field (S1BF), secondary somatosensory (S2), primary visual (V1) and auditory (A1) cortices. For each cortical region, two atlas-defined 2×2-voxel regions were chosen as the ipsilateral and contralateral seed, respectively. Seed locations are illustrated and shown in Fig. 2a and 5a. Reference signal profiles were generated by calculating the regionally averaged signals from the voxels within each seed. Pearson's correlation coefficients (CCs) were calculated between the reference signal profiles and the BOLD signals of every other voxel to generate individual correlation coefficient maps (CC maps) for each cortical region. Individual z-maps were then calculated from the corresponding CC maps using Fisher's Z transformation. Each group of z-maps per condition (e.g., z-maps of S1BF before optogenetic stimulation) were tested by a one sample *t*-test with FWE correction. This yielded the corresponding t statistics map for each condition (Supplementary Figs. 2a and c) to present only the significant connectivity ($P < 0.01$ for maps of S1BF, S2 and A1, $P < 0.02$ for maps of V1; FWE corrected). CC-threshold for group-averaged CC maps was set at $CC > 0.1$, corresponding to $P < 0.05$, to retain the features of the interhemispheric/bilateral functional connectivity networks in four sensory cortices detected by the t statistics maps (Supplementary Figs. 2a and c). The group-averaged rsfMRI functional connectivity maps (Figs. 2a and 5a, and Supplementary Figs. 2b and d) were generated by applying the CC-threshold on the group-averaged CC maps. The group-averaged rsfMRI functional connectivity maps were calculated for both the filtered (Figs. 2a and 5a, and Supplementary Figs. 3b and d) and non-filtered data (Supplementary Figs. 3a and c). Subsequently, 6×6-voxel regions of interest (ROIs) centered on each seed locations were then used to extract the CC values from the connectivity maps (e.g., contralateral S1BF ROI for maps generated using ipsilateral S1BF seed). Interhemispheric rsfMRI functional connectivity for each cortical region of filtered data was then quantified by averaging the CC values of the corresponding ipsilateral and contralateral ROI. Two-tail paired sample t tests were applied for both the z-scores (transformed from ROI-based CC values using Fisher's Z transformation) comparisons (Figs. 2b and 5b) and CC values comparisons (Supplementary Fig. 4). T statistics maps and group-averaged rsfMRI functional connectivity maps were also generated without global signal regression for the filtered data (Supplementary Fig. 5).

To examine the frequency components that contribute to the changes in the interhemispheric rsfMRI connectivity, intrahemispheric power spectrum and interhemispheric connectivity spectrum were generated for each cortical region from non-filtered rsfMRI signal profiles extracted from the respective ROIs. Standard MATLAB functions were used to calculate the power spectral density via Welch's method (0.005 Hz step-size) for intrahemispheric power spectrum, and magnitude-squared coherence (0.01 Hz step-size) for the interhemispheric connectivity spectrum. The observed increase or decrease in interhemispheric connectivity spectrum reflects the modulation effect on frequency-domain correlation between bilateral rsfMRI BOLD signals at specific frequency components (Chan et al., 2017; Nair et al., 2018). Quantifications of the interhemispheric connectivity spectrum and intrahemispheric power spectrum were made by integrating the areas under the curve before normalizing by the data points (i.e., steps defined in the spectra calculations within 0.01–0.1 Hz frequency range, not the power).

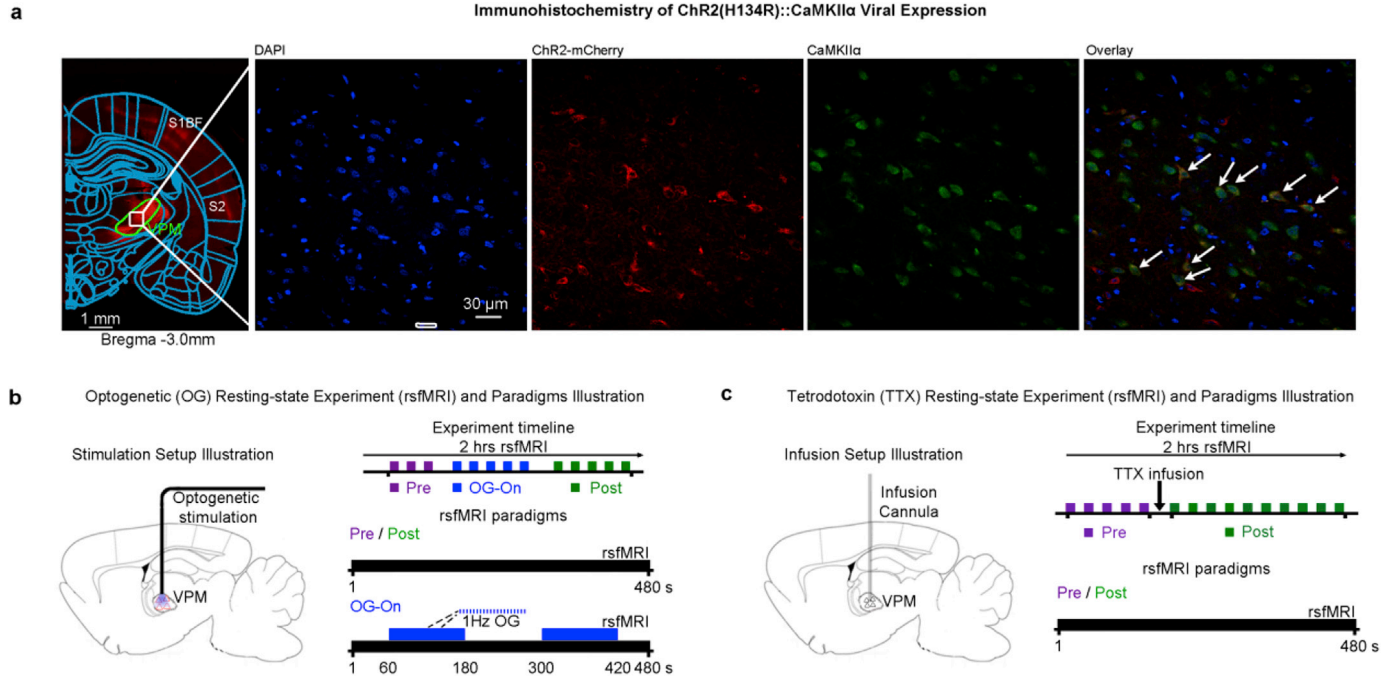

Fig. 1. Histological characterization of ChR2::CaMKIIα viral expression in ventral posteromedial (VPM) thalamocortical excitatory neurons and optogenetic/TTX rsfMRI experiment setup and paradigm. (**a**) Confocal images of ChR2-mCherry expression in VPM with lower magnification (Left) and higher magnification (Right). Overlay of images co-stained for the nuclear marker DAPI, excitatory marker CaMKIIα, and mCherry revealed colocalization of mCherry and CaMKIIα in the cell body of thalamo-cortical neurons (indicated by white arrows). (**b**) Illustration of optogenetic stimulation setup and experimental timeline (left) with 2 min on 2 min off 1 Hz optogenetic stimulation for an OG-On scan (right). (**c**) Illustration of TTX infusion setup (left), experimental timeline and a typical rsfMRI scan (right).

2.6. In vivo multi-depth electrophysiology experiments and data analyses

Multi-depth electrophysiological recordings were performed under the same anesthesia protocols and similar physiological conditions as in the rsfMRI experiments. Craniotomies were made and dura matter was removed with reference to the ROI regions of bilateral S1BF as in rsfMRI experiments. To cover cortical layers II/III to V/VI, two linear microelectrode silicon arrays (each array has 16 recording channels equally spaced at 100 μm; 1.5 MΩ impedance; NeuroNexus Technologies, Ann Arbor, MI) were inserted perpendicular to the cortical surface approximately 2.5 mm below the dura matter with micromanipulators (Narishige, Amityville, NY). Fiber implantation followed identical procedures as described for rsfMRI experiments. LFP data were acquired using a multi-channel neurophysiology recording system (sampling frequency: 24 kHz; notch-filter: 50 Hz, 100 Hz, and 150 Hz; Tucker Davis Technologies, Alachua, FL). Synchronized laser stimulation was controlled by the same system, and light pulses were recorded simultaneously with the neural data. Experiment paradigm was the same as used in rsfMRI experiments. After recordings, raw data were bandpass-filtered (0.01–150 Hz) and down-sampled to 1 kHz using Matlab.

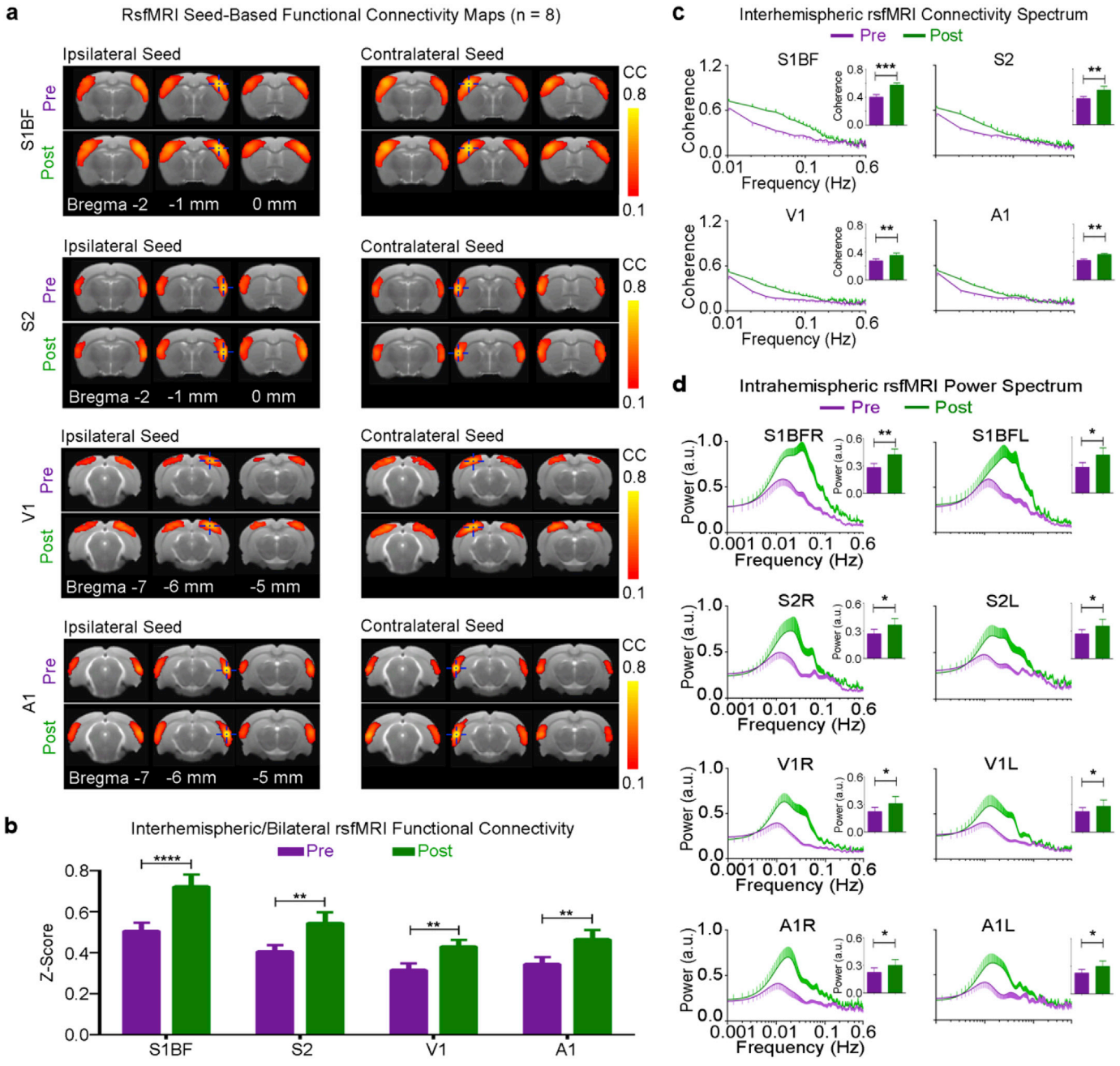

Fig. 2. rsfMRI connectivity in all sensory cortices are enhanced by low frequency optogenetic excitation of VPM thalamocortical excitatory neurons (n = 8). (**a**) Group-averaged functional connectivity maps of S1BF, S2, V1 and A1 before (pre) and after (post) low frequency (1 Hz) optogenetic stimulation of VPM thalamocortical excitatory neurons (n = 8; asterisk, stimulation site; blue crosshair indicates seed and ROI location). (**b**) ROI-based quantification for z-scores transformed from averaged interhemispheric connectivity correlation coefficient values using Fisher's Z transformation (n = 8; error bar indicates ± SEM, two-tail paired sample t tests; *** and **** denote $P < 0.001$ and $P < 0.0001$). (**c** and **d**) Interhemispheric rsfMRI connectivity spectrum and intrahemispheric rsfMRI power spectrum generated from the non-filtered rsfMRI signal. Area under the curve in each spectra were quantified and normalized by the frequency points across the 0.01–0.1 Hz range) for statistical analysis (n = 8; error bar indicates ± SEM, two-tail paired sample t tests; *, ** and *** denote $P < 0.05$, $P < 0.01$ and $P < 0.001$).

The relatively low spatial resolution of interhemispheric rsfMRI connectivity leads to the difficulty of examining the cortical layer involvement in the thalamic modulation effects. It is also difficult to infer the layer depths from multi-depth LFPs due to volume conductance. Current source density (CSD) analysis of the multi-depth LFPs allows a higher spatial resolution to identify the neural sources that contribute to the LFPs, and has been widely used in capturing the typical organization of sensory-evoked activity across cortical layers (Einevoll et al., 2013; Sakata and Harris, 2009). Typical sensory-evoked sink and source patterns span over the cortical layers and reflect the main excitatory drive of the thalamo-cortical and corpus callosum connections. In this study, we employed high resolution CSD analysis to identify cortical layers in our LFP data. In brief, CSDs were calculated as the second spatial derivative of LFPs and visualized by color-coded plots with linear interpolation (Einevoll et al., 2013; Quairiaux et al., 2011). Layer estimation and channel realignment for ipsilateral S1BF were performed upon determining the optogenetically evoked prominent primary CSD sinks at ~13 ms after stimulation onset in the middle channels and defining layer IV by the 4 channels covering the primary sink. For contralateral S1BF, after the appearance of the first sink (at ~19 ms), a triphasic CSD pattern (sink-source-sink covering layers II/III to V/VI) occurred between 25 and 50 ms. Here, the border between the sink in the upper channels and the source was used to define the lower boundary of layer IV. Other layers were then defined relative to the depth of layer IV. After channel realignment, each animal has fifteen channels covering the depths of bilateral S1BF with two channels for layer II/III, four channels for layer IV, and nine channels for layer V/VI.

To examine the effects of thalamic low frequency stimulation on cortical interhemispheric neural oscillations, intrahemispheric LFP power spectrum and interhemispheric LFP connectivity spectrum were computed for individual channels (see the Supplementary Fig. 6) before averaging across grouped layer-defined channels to generate the respective mean spectrum of each layer. Intrahemispheric LFP power spectra were the power spectral density calculated via Welch's method (0.05 Hz step-size). For interhemispheric connectivity spectrum, LFP data were first bandpass-filtered into individual frequency bands using a window size with a full width at half maximum (FWHM) of 0.1 Hz. Pearson's correlation coefficient was then calculated for each frequency band (Chan et al., 2017; J. M. Li et al., 2015). Peaks in the interhemispheric LFP connectivity spectrum indicate consistent correlation between bilateral LFP activities at the particular frequency range across animals. Quantification of all individual mean interhemispheric connectivity spectra was made based on the areas under the curve normalized by the data points within each traditionally defined frequency bands (ultra-slow: 0.1–0.5 Hz, slow: 0.5–1.5 Hz, delta: 1.5–4 Hz, theta: 4–8 Hz, alpha: 8–12 Hz, beta: 12–25 Hz, gamma: 25–100 Hz).

2.7. Histology, immunohistochemistry, and confocal imaging

To confirm the specific expression of ChR2-mCherry in the VPM excitatory neurons, histology was performed according to the previously published procedure (Chan et al., 2017; Leong et al., 2016). Upon completion of all rsfMRI and electrophysiological recording experiments, animals were anesthetized with pentobarbital and then transcardially perfused with ice-cold 4% para-formaldehyde (PFA) in phosphate buffered saline (PBS). The brains were equilibrated in 20% sucrose in PBS at 4 °C overnight. Axial sections (40 μm) were prepared on a freezing microtome (model 860, AO Scientific Instruments). Consecutive sections

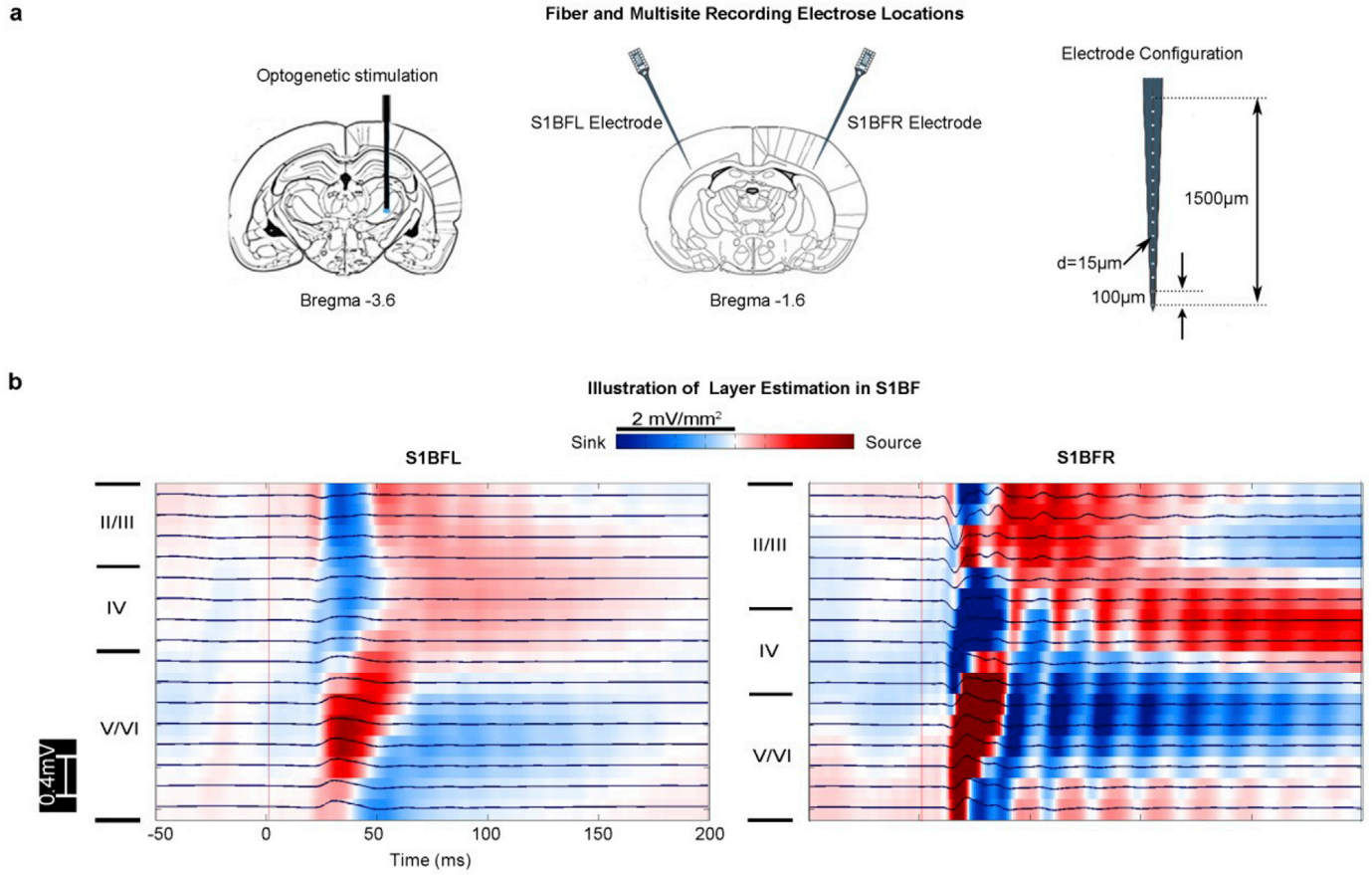

Fig. 3. Multi-depth cortical electrophysiology recording setup, representative traces during optogenetic stimulation. (**a**) Illustration of multi-depth recording electrodes locations for the electrophysiology experiment. (**b**) Representative local field potential (LFP) traces in black during optogenetic stimulation (red line represents the stimulation onset) overlaid on the current source density (CSD) maps. Note that the CSD analysis was performed here to facilitate the identification and realignment of bilateral somatosensory cortical layers for subsequent interhemispheric and intrahemispheric LFP analyses.

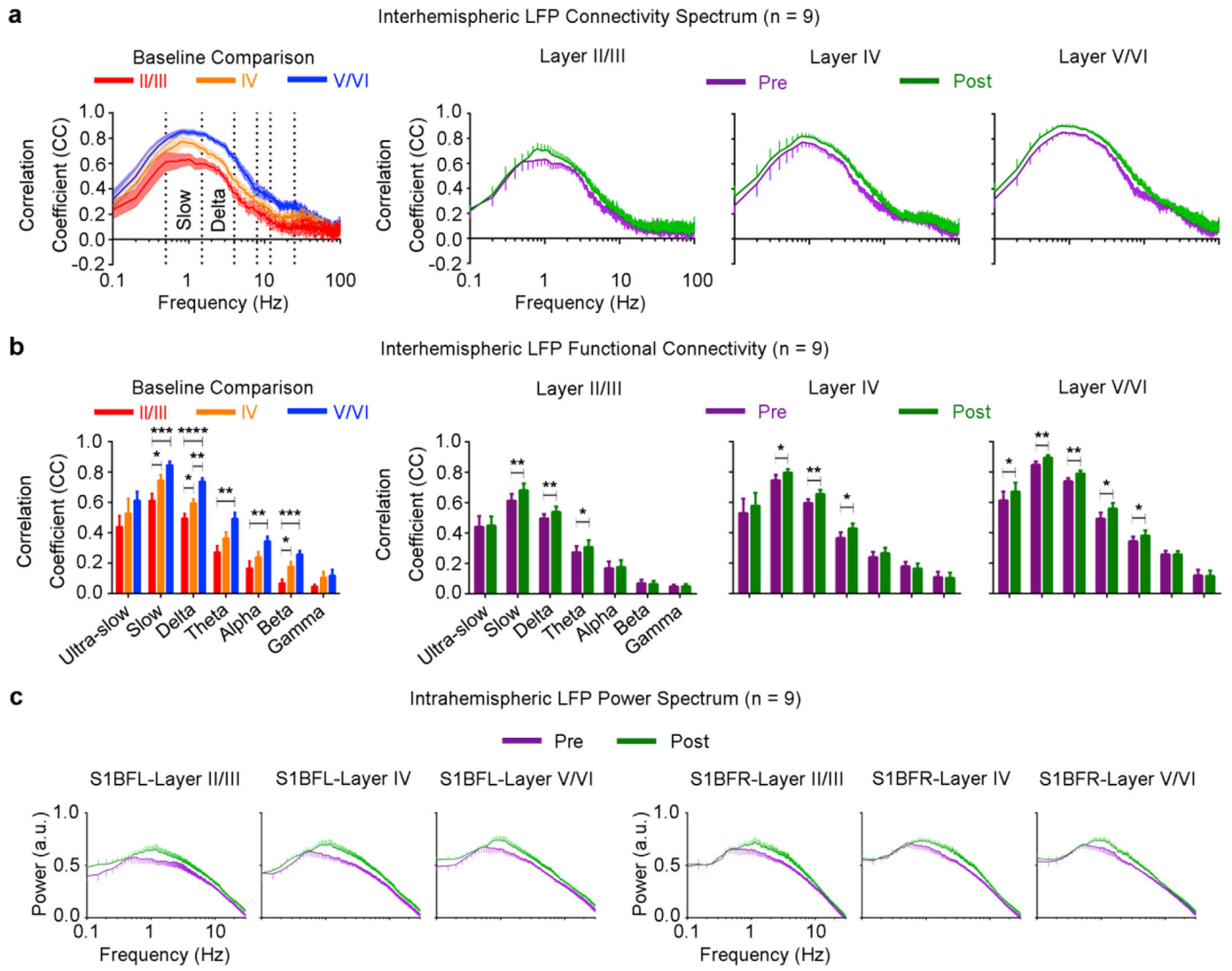

Fig. 4. Interhemispheric LFP connectivity and intrahemispheric LFP power of low frequency neural oscillations at all cortical layers were elevated by low frequency (1 Hz) optogenetic stimulation of VPM thalamocortical excitatory neurons (n = 9). (**a**) Interhemispheric correlation between bilateral S1BF was increased in slow, delta and theta oscillations across all layers after optogenetic stimulation. (**b**) Statistical analysis of averaged interhemispheric LFP connectivity across different defined frequency bands and cortical layers (ultra-slow: 0.1–0.5 Hz, slow: 0.5–1.5 Hz, delta: 1.5–4 Hz, theta: 4–8 Hz, alpha: 8–12 Hz, beta: 12–25 Hz, gamma: 25–100 Hz). One-way ANOVAs with post-hoc corrections were employed for baseline comparison. Two-tail paired sample t tests were used for the comparisons between pre and post optogenetic stimulation. Error bar indicates ± SEM (*, **, ***, and **** denotes $P < 0.05$, $P < 0.01$, $P < 0.001$, and $P < 0.0001$). (**c**) All layers showed the increase of intrahemispheric resting-state LFP power in slow and delta oscillations after optogenetic stimulation.

were mounted and examined with a laser confocal microscope (Carl Zeiss LSM780). For immunohistochemistry, free-floating sections were processed with 5% normal goat serum and 0.3% Triton X-100 in PBS with primary antibodies against rabbit polyclonal to CaMKIIα (1:400; Abcam) at 4 °C for 24 h. After washing with PBS, sections were then incubated for 2 h at room temperature with secondary antibodies Alexa Fluor 647 conjugate goat anti-rabbit IgG and Alexa Fluor 488 conjugate goat anti-guinea pig IgG (both 1:500; Molecular Probe). Slices were then washed and mounted using FluoroShield mounting medium with DAPI (Abcam). Double or triple immunofluorescence was assessed with a laser confocal microscope (Carl Zeiss LSM780).

3. Results

3.1. Optogenetic stimulation of VPM thalamocortical excitatory neurons increases brain-wide cortical interhemispheric rsfMRI connectivity

After confirming the specific expression of ChR2-mCherry in VPM thalamocortical excitatory neurons through colocalization of mCherry with CaMKIIα staining (Fig. 1a), we examined the modulatory effects of thalamic low frequency optogenetic stimulation on interhemispheric rsfMRI connectivity in lightly anesthetized rats (Fig. 1b). We found that after (post) 1 Hz VPM stimulation, the strength of interhemispheric rsfMRI connectivity increased significantly in primary somatosensory barrel field (S1BF), secondary somatosensory cortex (S2), primary visual cortex (V1) and primary auditory cortex (A1) (Figs. 2a and b; n = 8; S1BF: 42.7 ± 4.4%, $P < 0.0001$; S2: 34.0 ± 9.1%, $P < 0.01$; V1: 35.5 ± 5.6%, $P < 0.01$; and A1: 31.3 ± 4.3%, $P < 0.01$; two-tail paired sample *t*-test). These findings demonstrate that optogenetic stimulation modulates the strength of interhemispheric rsfMRI connectivity of multiple sensory cortices.

To determine the frequency components that contribute to the enhanced interhemispheric rsfMRI connectivity, we calculated the interhemispheric connectivity spectrum and intrahemispheric/local power spectrum of rsfMRI BOLD activity. We observed significantly enhanced interhemispheric connectivity of infraslow (0.01–0.1 Hz)

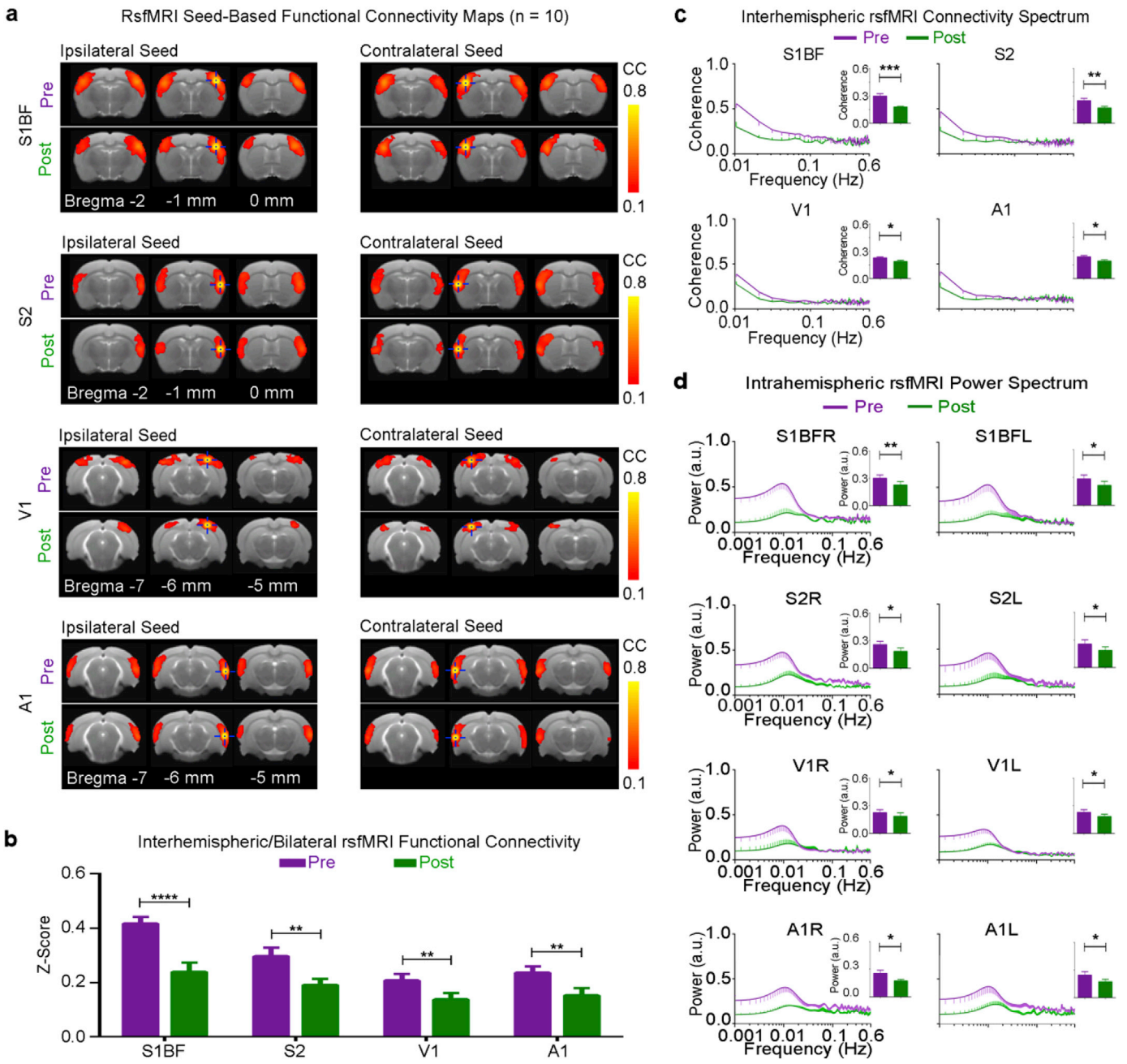

Fig. 5. Tetrodotoxin (TTX) inhibition of VPM thalamocortical neurons decreased interhemispheric rsfMRI connectivity in sensory cortices. (a) Group-averaged rsfMRI functional connectivity maps of S1BF, S2, V1 and A1 before and after TTX infusion into VPM thalamocortical neurons (n = 10; asterisk, infusion site; blue crosshair indicates seed and ROI location). (b) ROI-based quantification for z-scores transformed from averaged interhemispheric connectivity correlation coefficient values using Fisher's Z transformation (n = 10; error bar indicates ± SEM, two-tail paired sample t tests; *, ** and *** denote $P < 0.05$, $P < 0.01$ and $P < 0.001$). (c and d) Interhemispheric rsfMRI connectivity spectrum and intrahemispheric rsfMRI power spectrum generated from the non-filtered rsfMRI signal. Area under the curve in each spectrum was quantified and normalized by the frequency points across the 0.01–0.1 Hz range) for statistical analysis (n = 10; error bar indicates ± SEM, two-tail paired sample t tests; *, ** and *** denote $P < 0.05$, $P < 0.01$ and $P < 0.001$).

rsfMRI BOLD activity post stimulation (Fig. 2c; n = 8; S1BF: 43.1 ± 6.7%, $P < 0.001$; S2: 32.9 ± 6.8%, $P < 0.01$; V1: 28.9 ± 7.7%, $P < 0.01$; and A1: 31.8 ± 6.2%, $P < 0.01$; two-tail paired sample t tests). We also observed a significant enhancement in the strength of intrahemispheric rsfMRI BOLD activity at infraslow (0.01–0.1 Hz) frequency post stimulation (Fig. 2d; n = 8; S1BFR: 51.2 ± 9.3%, $P < 0.01$; S1BFL: 47.8 ± 17.3%, $P < 0.05$; S2R: 35.7 ± 14.3%, $P < 0.05$; S2L: 31.7 ± 10.7%, $P < 0.05$; V1R: 34.9 ± 15.6%, $P < 0.05$; V1L: 27.2 ± 17.9%, $P < 0.05$; A1R: 34.8 ± 10.2%, $P < 0.05$; and A1L: 31.8 ± 16.6%, $P < 0.05$; two-tail paired sample t tests). These results demonstrate that both the enhanced interhemispheric coherence and intrahemispheric strength of the infraslow (0.01–0.1 Hz) BOLD activity at bilateral sensory cortices contribute to enhanced cortical interhemispheric rsfMRI connectivity. These findings demonstrate that low frequency somatosensory thalamic activity modulates brain-wide interhemispheric rsfMRI connectivity beyond its sensory modality.

3.2. Optogenetic stimulation of VPM thalamocortical excitatory neurons increases cortical interhemispheric LFP connectivity of low frequency neural oscillations in all cortical layers

To further examine the neural activities that underlie the

enhancement of cortical interhemispheric rsfMRI connectivity, we performed multi-depth LFP recordings covering the supragranular (layer II/III), granular (layer IV) and infragranular (layer V/VI) layers of bilateral S1BF (Fig. 3a) pre and post 1 Hz optogenetic stimulation of VPM excitatory neurons.

After recordings in the pre-stimulation stage, we confirmed the recording location and performed layer estimation by analyzing the sink-source patterns in the CSD maps of evoked LFPs (Fig. 3b). We observed that in the ipsilateral cortex (S1BFR), the primary sink started at ~13 ms in layer IV (middle channels) and propagated to layer II/III (upper channels) and layer V/VI (deeper channels). In the contralateral cortex (S1BFL), the first sink started at ~19 ms in layer V and propagated to layer IV and layer II/III. These results confirmed the typical CSD patterns of evoked LFPs within cortical layers and between bilateral cortices (Boorman et al., 2010; Quairiaux et al., 2011), which corroborated the documented conduction delays of neural activity through direct thalamo-cortical connections and interhemispheric corpus callosum connections (Debanne et al., 2011; Leong et al., 2016; Quairiaux et al., 2011).

We then examined the effects of 1 Hz optogenetic stimulation on the interhemispheric connectivity spectrum and intrahemispheric power spectrum of resting-state LFPs at each cortical layer. Although the deeper layers showed stronger interhemispheric LFP connectivity than the upper layers pre-stimulation (Figs. 4a and b), interhemispheric connectivity strengthened significantly at all cortical layers post stimulation, particularly the correlation of slow, delta and theta oscillations (Figs. 4a and b; $n = 9$; Layer II/III: slow, $11.1 \pm 2.4\%$, $P < 0.01$; delta, $8.4 \pm 2.3\%$, $P < 0.01$; theta, $12.7 \pm 5.0\%$, $P < 0.05$; Layer IV: slow, $6.7 \pm 2.4\%$, $P < 0.05$; delta, $10.1 \pm 2.9\%$, $P < 0.01$; theta, $17.4 \pm 6.6\%$, $P < 0.05$; Layer V/VI: ultra-slow, $9.4 \pm 4.2\%$, $P < 0.05$; slow, $5.5 \pm 1.4\%$, $P < 0.01$; delta, $6.8 \pm 1.9\%$, $P < 0.01$; theta, $13.5 \pm 4.9\%$, $P < 0.05$; alpha, $10.8 \pm 5.3\%$, $P < 0.05$; two-tail paired sample t tests). We also observed an increase in the intrahemispheric LFP power of slow, delta and theta oscillations at all layers of bilateral S1BF post stimulation. These results demonstrate that thalamic stimulation increased interhemispheric cortical low frequency neural oscillations (i.e., mainly slow oscillations at 0.5–1.5 Hz, delta oscillations at 1.5–4 Hz and theta oscillations at 4–8 Hz), which may underlie the enhancement found in cortical interhemispheric rsfMRI connectivity. Further, they suggest that low frequency neural oscillations in all cortical layers contribute to enhanced cortical interhemispheric rsfMRI connectivity.

3.3. Pharmacological inhibition of VPM thalamocortical neurons decreases brain-wide cortical interhemispheric rsfMRI connectivity

To complement the optogenetic rsfMRI experiments, we pharmacologically inhibited VPM thalamocortical neurons with TTX to examine the effect on interhemispheric rsfMRI. RsfMRI was acquired before (pre) and after (post) infusion of TTX (Fig. 5a). Pharmacological inhibition weakened the spatial extent and strength of interhemispheric rsfMRI connectivity in S1BF, S2, V1, and A1 (Figs. 5a and b; $n = 10$; S1BF: $-42.6 \pm 7.5\%$, $P < 0.0001$; S2: $-35.6 \pm 6.3\%$, $P < 0.01$; V1: $-33.6 \pm 6.2\%$, $P < 0.01$; and A1: $-35.4 \pm 7.9\%$, $P < 0.01$; two-tail paired sample t tests). The interhemispheric rsfMRI connectivity spectra showed a significant decrease in the infraslow (0.01–0.1 Hz) frequency post TTX infusion (Fig. 5c; $n = 10$; S1BF: $-39.8 \pm 6.0\%$, $P < 0.001$; S2: $-32.5 \pm 6.1\%$, $P < 0.01$; V1: $26.3 \pm 4.7\%$, $P < 0.05$; and A1: $28.3 \pm 7.3\%$, $P < 0.05$; two-tail paired sample t tests). We also observed a significant decrease in infraslow (0.01–0.1 Hz) intrahemispheric rsfMRI BOLD activity post TTX infusion (Fig. 5d; $n = 10$; S1BFR: $-30.7 \pm 5.1\%$, $P < 0.01$; S1BFL: $-29.0 \pm 7.7\%$, $P < 0.05$; S2R: $-26.3 \pm 5.2\%$, $P < 0.05$; S2L: $-25.4 \pm 6.6\%$, $P < 0.05$; V1R: $-19.9 \pm 5.6\%$, $P < 0.05$; V1L: $-20.4 \pm 5.0\%$, $P < 0.05$; A1R: $-23.9 \pm 4.9\%$, $P < 0.05$; and A1L: $-24.2 \pm 5.5\%$, $P < 0.05$; two-tail paired sample t tests). Combined with the results of optogenetic rsfMRI experiments, these findings demonstrate that the thalamus is a pivotal subcortical region that directly contributes to brain-wide rsfMRI connectivity.

4. Discussion

In summary, we directly reveal the pivotal contribution of the thalamus to brain-wide interhemispheric rsfMRI connectivity. Our findings demonstrated that thalamically-evoked low frequency activity by optogenetic stimulation of VPM thalamocortical excitatory neurons increased interhemispheric rsfMRI connectivity and local cortical intrahemispheric BOLD activity in all sensory cortices at infraslow frequency 0.01–0.1 Hz. In parallel, our electrophysiological recordings after low frequency (1 Hz) optogenetic stimulation of VPM revealed increased cortical interhemispheric correlation at low frequency neural oscillations (mainly < 10 Hz) and local cortical oscillations in all cortical layers. Meanwhile, pharmacological inhibition of VPM thalamocortical neurons decreased brain-wide cortical interhemispheric rsfMRI connectivity and local cortical intrahemispheric BOLD activity. Together, these results demonstrate that low frequency activities in the thalamo-cortical network modulate brain-wide cortical interhemispheric rsfMRI connectivity. These results highlight the key contributions of thalamus to brain-wide rsfMRI connectivity.

4.1. Thalamus contributes to brain-wide interhemispheric resting-state functional MRI connectivity

Although emerging evidence supports that thalamus mediates diverse functional neural integrations involved in cortical processing (Hwang et al., 2017; Rikhye et al., 2018; Sherman, 2016), a direct role for thalamus in cortical rsfMRI connectivity remains elusive, since few studies if any directly interrogate thalamic contributions to brain-wide rsfMRI connectivity. In the present study, low frequency (1 Hz) optogenetic stimulation of sensory thalamus enhanced brain-wide cortical interhemispheric and intrahemispheric rsfMRI connectivity, whereas TTX pharmacological inhibition of sensory thalamus induced an opposite effect. Note that TTX inhibition has larger effects than optogenetic stimulation on the 0.001–0.01 Hz rsfMRI BOLD activity. This likely arises from the broad effects of TTX non-cell-type-specific sodium channel blocking in inhibiting thalamic neuronal and astrocytic <0.01 Hz infraslow electrophysiological oscillations (Copeland et al., 2017; S. W. Hughes et al., 2011; Lorincz et al., 2009; Pappalardo et al., 2016), and cortical <15 Hz electrophysiological oscillations (David et al., 2013; Liu et al., 2018; Schölvinck et al., 2010; L. Yan et al., 2009). The observed changes in cortical rsfMRI connectivity that initiated from VPM do not preclude the potential contributions from: (1) other thalamic nuclei (e.g., posterior medial nucleus and non-somatosensory thalamus), which are connected to VPM through either the cortex or thalamic reticular nucleus (Halassa et al., 2014; Lam and Sherman, 2007, 2011; Lewis et al., 2015); (2) intact monosynaptic interhemispheric corpus callosum connections (O'Reilly et al., 2013; Roland et al., 2017; Zhou et al., 2014) and polysynaptic connections through anterior or posterior commissure (O'Reilly et al., 2013; Roland et al., 2017; Tovar-Moll et al., 2014); and (3) other critical subcortical regions such as hippocampus (Chan et al., 2017), basal forebrain (Liu et al., 2018; Turchi et al., 2018), and striatum (Albaugh et al., 2016). Nevertheless, these findings directly demonstrate that brain-wide cortical interhemispheric rsfMRI connectivity strongly depends on thalamic inputs, specifically the sensory thalamus. Moreover, the present results also suggest that the dynamic changes that have been observed in cortical rsfMRI connectivity when one is subjected to different cognitive tasks (Park and Friston, 2013) can be supported and/or influenced by thalamic inputs. Such findings may arise from the ability of the sensory thalamus to initiate brain-wide polysynaptic interactions with the cortex (Leong et al., 2016; Xiao et al., 2017).

Multiple independent lines of evidence suggest that thalamus influences brain-wide rsfMRI connectivity through polysynaptic connections and long-range coupling of low frequency neural oscillations (mainly < 10 Hz). Thalamic-related ascending subcortical

neuromodulatory inputs have been proposed to increase long-range synchrony of spontaneous slow oscillations (Fernandez et al., 2017; Gent et al., 2018; Olcese et al., 2016). Other studies using multisite electrophysiology (Sheroziya and Timofeev, 2014), voltage-dependent-dye (Mohajerani et al., 2013) and calcium imaging (Xiao et al., 2017) have also demonstrated an essential role for thalamic activity in shaping and maintaining brain-wide dynamics of cortical slow activities (<5 Hz). By analyzing the correlation between arousal-dependent fluctuations in neural activity and brain-wide fMRI BOLD signals, recent studies observed indirect thalamic involvement in regulating spontaneous brain-wide rsfMRI BOLD activity through subcortical neuromodulatory pathways (Chang et al., 2016; Liu et al., 2018; Schölvinck et al., 2010; Turchi et al., 2018). Our recent investigation using fMRI and electrophysiological recordings demonstrated that low, not high, frequency stimulation of VPM excitatory thalamocortical neurons initiated robust propagation of slow activity to all sensory cortices, likely through recruiting reciprocal interactions over thalamo-cortico-thalamic, cortico-cortical and interhemispheric corpus callosum connections (Leong et al., 2016). The present results provide further evidence for engaging polysynaptic inter-layer and cross-modal cortico-cortical connections. More importantly, our findings provide direct evidence on the contributions of low frequency neural oscillations in thalamo-cortical networks to brain-wide rsfMRI connectivity.

4.2. Polysynaptic inter-layer cortical and cross-modal cortical connections in brain-wide interhemispheric resting-state functional MRI connectivity

The contributions of polysynaptic connections to cortical interhemispheric rsfMRI connectivity have been indicated by studies showing that cortical interhemispheric rsfMRI connectivity can vary due to subcortical perturbations (Chan et al., 2017) or largely preserved after corpus callosum lesions (O'Reilly et al., 2013; Roland et al., 2017; Tyszka et al., 2011; Zhou et al., 2014). However, little evidence exists to confirm and characterize such contributions. We find that despite the somatosensory cortical layer V/VI exhibiting the strongest interhemispheric LFP connectivity at baseline, the interhemispheric correlations of low frequency neural oscillations at all layers were enhanced after thalamic stimulation. The initial modulatory effects from VPM on low frequency cortical neural oscillations likely occur at the deeper layers of S1BF, which are considered as the site of initiation for slow oscillations (S. Hughes and Crunelli, 2013; Lorincz et al., 2015; Sakata and Harris, 2009), and at layers II/III and V/VI, which are the dominant sites for interhemispheric corpus callosum connections (Baek et al., 2016; Honey et al., 2009). Importantly, our rsfMRI and electrophysiology results indicate that these initial thalamic effects subsequently spread across other cortical layers through their polysynaptic inter-layer connections. Recruiting multiple cortical layers polysynaptically could be a common feature underlying all cortical rsfMRI connectivity, including non-interhemispheric rsfMRI connectivity like inter-regional rsfMRI connectivity between sensory cortices that relies less on corpus callosum connections.

Since cross-modal interactions are essential for sensory processing, they have been studied extensively under task conditions using fMRI and other neuroimaging methods (Ibrahim et al., 2016; Kok et al., 2012; F. Liang et al., 2015; M. Liang et al., 2013). However, less is known about cross-modal interactions of spontaneous activity during rest. These interactions may be important to prepare long-range brain-wide networks to process multisensory information. Using low frequency optogenetic stimulation or pharmacological inhibition, the present results demonstrate that cortical interhemispheric rsfMRI connectivity beyond the somatosensory modality could be modulated by somatosensory thalamus. Based on our fMRI and electrophysiology findings, we suggest that thalamically-evoked low frequency activity recruits cross-modal connections polysynaptically, which subsequently elevates the interhemispheric synchrony of low frequency oscillations in other sensory cortices. Indeed, our previous study showed that low frequency stimulation of VPM evoked BOLD activations in bilateral V1, A1 and S2 (Leong et al., 2016). The evoked LFPs in bilateral S1 and V1 showed persistent neural activity lasting for 200–300 ms, which draws similarities to spontaneous cortical slow oscillations (Sheroziya and Timofeev, 2014; Stroh et al., 2013). The most probable pathways for these cross-modal interactions are the cortico-cortical connections between somatosensory cortices and visual/auditory cortices (Sieben et al., 2013; Zingg et al., 2014). This is supported by our previous study showing that the latency of the optogenetically evoked LFPs between S1 and V1 is in line with the typical axonal conduction time for the corresponding cortico-cortical connections (Leong et al., 2016). Sparse direct thalamo-cortical connections between VPM and V1/A1 and cortico-thalamo-cortical connections through other thalamic nuclei can also be possible pathways underlying such cross-modal interactions (Budinger and Scheich, 2009; Cappe et al., 2012; Henschke et al., 2015). Taken together, somatosensory thalamic low frequency activity likely modulates low frequency cortical cross-modal interactions and neural oscillations, from which changes in the interhemispheric rsfMRI connectivity in other sensory cortices emerge.

Based on the above discussions and the cortical interhemispheric LFP connectivity changes observed across multiple cortical layers, we suggest that the cortico-cortical pathway is likely the predominant pathway recruited by VPM to mediate brain-wide rsfMRI connectivity. Other thalamic nuclei are also connected to VPM via reticular thalamic nucleus (Halassa et al., 2014; Lam and Sherman, 2007, 2011; Lewis et al., 2015). Although the density and properties of such thalamo-thalamic connections remain to be further studied, they may support VPM to drive other thalamic nuclei and subsequently recruit cortico-cortical pathway to mediate cortical interhemispheric rsfMRI connectivity. Therefore, our current study cannot preclude the potential contributions from the thalamo-thalamic pathway.

4.3. Low frequency neural oscillations in the thalamo-cortical network underlying resting-state functional MRI connectivity

Our results here indicate that slow (0.5–1.5 Hz) and delta (1.5–4 Hz) oscillations could be the neural correlates of rsfMRI BOLD signals and that thalamic inputs could shape their interhemispheric correlation. A recent study (Ma et al., 2016) using calcium imaging showed that the infraslow resting-state hemodynamic activity in the anesthetized and awake brain was coupled to slow and delta oscillations-associated neuronal calcium activities. Moreover, a rsfMRI study (Schwalm et al., 2017) also showed that such slow and delta oscillations-associated calcium activities correlated to brain-wide infraslow BOLD activity during rest. Although it is unclear how the infraslow BOLD activity is coupled to the slow and delta oscillations, our results demonstrate a close relationship. Both oscillations were directly influenced by the thalamus and paralleled the changes observed in cortical interhemispheric rsfMRI connectivity.

The present study also showed an increase in theta (4–8 Hz) and alpha (8–12 Hz) oscillations, which could implicate spindle oscillations that originate from the thalamus (Astori et al., 2013; McCormick et al., 2015). Given the tight interactions between spindle, and slow and/or delta oscillations (Mak-McCully et al., 2017), changes in slow oscillations could accompany corresponding changes in spindle oscillations. Our electrophysiology results corroborated the findings from two studies, which showed that slow and spindle oscillations in the thalamic-cortical network were both modulated after pharmacologically inhibiting VPM thalamocortical neurons (David et al., 2013) or during the transition between sleep-wake cycles (Fernandez et al., 2017). Taken together, our findings suggest that cross-frequency coupling between slow and spindle oscillations may support rsfMRI connectivity.

4.4. Conclusion

In summary, our results demonstrate that low frequency somatosensory thalamic activity contributes to cortical interhemispheric rsfMRI

connectivity within and across the sensory modality. We propose this occurs through recruiting interhemispheric low frequency neural oscillations in all cortical layers and engaging polysynaptic connections in the thalamo-cortical network. Our findings indicate that the thalamus plays a more significant role beyond its traditional view as a relay station, especially given its contribution to brain-wide rsfMRI functional connectivity.

Acknowledgements

This work was supported by the Hong Kong Research Grant Council (C7048-16G to E.X.W.), Guangdong Provincial Brain Research Key Projects (No. 2018B030332001 and No. 2018B030336001), and Lam Woo Foundation. We would also like to thank Dr. K. Deisseroth who provided us with the ChR2 viral construct.

Appendix A. Supplementary data

Supplementary data to this article can be found online at https://doi.org/10.1016/j.neuroimage.2019.06.063.

Conflicts of interest

The authors declare that they have no competing financial interests.

Author contributions

This study was conceived and designed by E.X.W., X.W., and A.T.L.L. The animal surgery was conducted by X.W. All rsfMRI experiments were performed by X.W. and A.T.L.L. Data were analyzed by X.W., R.W.C., A.T.L.L., Y. L and E.X.W. The results were discussed by all authors. The manuscript was written by X.W., A.T.L.L. and E.X.W.

References

Albaugh, D.L., Salzwedel, A., Van Den Berge, N., Gao, W., Stuber, G.D., Shih, Y.-Y.I., 2016. Functional magnetic resonance imaging of electrical and optogenetic deep brain stimulation at the rat nucleus accumbens. Sci. Rep. 6, 31613. https://doi.org/10.1038/srep31613 (2016).

Alonso, J.M., Swadlow, H.A., 2015. Thalamus controls recurrent cortical dynamics. Nat. Neurosci. 18 (12), 1703–1704. https://doi.org/10.1038/nn.4175.

Astori, S., Wimmer, R.D., Luthi, A., 2013. Manipulating sleep spindles–expanding views on sleep, memory, and disease. Trends Neurosci. 36 (12), 738–748. https://doi.org/10.1016/j.tins.2013.10.001.

Baek, K., Shim, W.H., Jeong, J., Radhakrishnan, H., Rosen, B.R., Boas, D., Franceschini, M., Biswal, B.B., Kim, Y.R., 2016. Layer-specific interhemispheric functional connectivity in the somatosensory cortex of rats: resting state electrophysiology and fMRI studies. Brain Struct. Funct. 221 (5), 2801–2815. https://doi.org/10.1007/s00429-015-1073-0.

Birn, R.M., 2012. The role of physiological noise in resting-state functional connectivity. Neuroimage 62 (2), 864–870. https://doi.org/10.1016/j.neuroimage.2012.01.016.

Biswal, B., Zerrin Yetkin, F., Haughton, V.M., Hyde, J.S., 1995. Functional connectivity in the motor cortex of resting human brain using echo-planar MRI. Magn. Reson. Med. 34 (4), 537–541. https://doi.org/10.1002/mrm.1910340409.

Boorman, L., Kennerley, A.J., Johnston, D., Jones, M., Zheng, Y., Redgrave, P., Berwick, J., 2010. Negative blood oxygen level dependence in the rat: a model for investigating the role of suppression in neurovascular coupling. J. Neurosci. 30 (12), 4285–4294. https://doi.org/10.1523/JNEUROSCI.6063-09.2010.

Budinger, E., Scheich, H., 2009. Anatomical connections suitable for the direct processing of neuronal information of different modalities via the rodent primary auditory cortex. Hear. Res. 258 (1–2), 16–27. https://doi.org/10.1016/j.heares.2009.04.021.

Cappe, C., Rouiller, E.M., Barone, P., 2012. Cortical and thalamic pathways for multisensory and sensorimotor interplay. In: Murray, M.M., Wallace, M.T. (Eds.), The Neural Bases of Multisensory Processes. CRC Press, Boca Raton (FL), pp. 13–28.

Chan, R.W., Leong, A.T., Ho, L.C., Gao, P.P., Wong, E.C., Dong, C.M., Wang, X., He, J., Chan, Y.-S., Lim, L.W., Wu, E.X., 2017. Low-frequency hippocampal–cortical activity drives brain-wide resting-state functional MRI connectivity. Proc. Natl. Acad. Sci. Unit. States Am. 114 (33), E6972–E6981. https://doi.org/10.1073/pnas.1703309114.

Chang, C., Leopold, D.A., Schölvinck, M.L., Mandelkow, H., Picchioni, D., Liu, X., Frank, Q.Y., Turchi, J.N., Duyn, J.H., 2016. Tracking brain arousal fluctuations with fMRI. Proc. Natl. Acad. Sci. Unit. States Am. 113 (16), 4518–4523. https://doi.org/10.1073/pnas.1520613113.

Chuang, K.H., Nasrallah, F.A., 2017. Functional networks and network perturbations in rodents. Neuroimage 163, 419–436. https://doi.org/10.1016/j.neuroimage.2017.09.038.

Cole, M.W., Ito, T., Bassett, D.S., Schultz, D.H., 2016. Activity flow over resting-state networks shapes cognitive task activations. Nat. Neurosci. 19 (12), 1718–1726. https://doi.org/10.1038/nn.4406.

Cole, M.W., Pathak, S., Schneider, W., 2010. Identifying the brain's most globally connected regions. Neuroimage 49 (4), 3132–3148. https://doi.org/10.1016/j.neuroimage.2009.11.001.

Constantinople, C.M., Bruno, R.M., 2013. Deep cortical layers are activated directly by thalamus. Science 340 (6140), 1591–1594. https://doi.org/10.1126/science.1236425.

Copeland, C., Wall, T., Sims, R., Neale, S., Nisenbaum, E., Parri, H., Salt, T., 2017. Astrocytes modulate thalamic sensory processing via mGlu2 receptor activation. Neuropharmacology 121, 100–110. https://doi.org/10.1016/j.neuropharm.2017.04.019.

Crossley, N.A., Mechelli, A., Vertes, P.E., Winton-Brown, T.T., Patel, A.X., Ginestet, C.E., McGuire, P., Bullmore, E.T., 2013. Cognitive relevance of the community structure of the human brain functional coactivation network. Proc. Natl. Acad. Sci. Unit. States Am. 110 (28), 11583–11588. https://doi.org/10.1073/pnas.1220826110.

Cruikshank, S.J., Urabe, H., Nurmikko, A.V., Connors, B.W., 2010. Pathway-specific feedforward circuits between thalamus and neocortex revealed by selective optical stimulation of axons. Neuron 65 (2), 230–245. https://doi.org/10.1016/j.neuron.2009.12.025.

Crunelli, V., David, F., Lorincz, M.L., Hughes, S.W., 2015. The thalamocortical network as a single slow wave-generating unit. Curr. Opin. Neurobiol. 31, 72–80. https://doi.org/10.1016/j.conb.2014.09.001.

David, F., Schmiedt, J.T., Taylor, H.L., Orban, G., Di Giovanni, G., Uebele, V.N., Renger, J.J., Lambert, R.C., Leresche, N., Crunelli, V., 2013. Essential thalamic contribution to slow waves of natural sleep. J. Neurosci. 33 (50), 19599–19610. https://doi.org/10.1523/JNEUROSCI.3169-13.2013.

Debanne, D., Campanac, E., Bialowas, A., Carlier, E., Alcaraz, G., 2011. Axon physiology. Physiol. Rev. 91 (2), 555–602. https://doi.org/10.1152/physrev.00048.2009.

Douglas, R.J., Martin, K.A., 2004. Neuronal circuits of the neocortex. Annu. Rev. Neurosci. 27, 419–451. https://doi.org/10.1146/annurev.neuro.27.070203.144152.

Drysdale, A.T., Grosenick, L., Downar, J., Dunlop, K., Mansouri, F., Meng, Y., Fetcho, R.N., Zebley, B., Oathes, D.J., Etkin, A., Schatzberg, A.F., Sudheimer, K., Keller, J., Mayberg, H.S., Gunning, F.M., Alexopoulos, G.S., Fox, M.D., Pascual-Leone, A., Voss, H.U., Casey, B.J., Dubin, M.J., Liston, C., 2017. Resting-state connectivity biomarkers define neurophysiological subtypes of depression. Nat. Med. 23 (1), 28–38. https://doi.org/10.1038/nm.4246.

Dudai, Y., Karni, A., Born, J., 2015. The consolidation and transformation of memory. Neuron 88 (1), 20–32. https://doi.org/10.1016/j.neuron.2015.09.004.

Einevoll, G.T., Kayser, C., Logothetis, N.K., Panzeri, S., 2013. Modelling and analysis of local field potentials for studying the function of cortical circuits. Nat. Rev. Neurosci. 14 (11), 770–785. https://doi.org/10.1038/nrn3599.

Feldmeyer, D., 2012. Excitatory neuronal connectivity in the barrel cortex. Front. Neuroanat. 6, 24. https://doi.org/10.3389/fnana.2012.00024.

Fernandez, L.M.J., Comte, J.C., Le Merre, P., Lin, J.S., Salin, P.A., Crochet, S., 2017. Highly dynamic spatiotemporal organization of low-frequency activities during behavioral states in the mouse cerebral cortex. Cerebr. Cortex 27 (12), 5444–5462. https://doi.org/10.1093/cercor/bhw311.

Fox, M.D., Raichle, M.E., 2007. Spontaneous fluctuations in brain activity observed with functional magnetic resonance imaging. Nat. Rev. Neurosci. 8 (9), 700–711. https://doi.org/10.1038/nrn2201.

Fox, M.D., Zhang, D., Snyder, A.Z., Raichle, M.E., 2009. The global signal and observed anticorrelated resting state brain networks. J. Neurophysiol. 101 (6), 3270–3283. https://doi.org/10.1152/jn.90777.2008.

Gent, T.C., Bandarabadi, M., Herrera, C.G., Adamantidis, A.R., 2018. Thalamic dual control of sleep and wakefulness. Nat. Neurosci. 21 (7), 974–984. https://doi.org/10.1038/s41593-018-0164-7.

Halassa, M.M., Chen, Z., Wimmer, R.D., Brunetti, P.M., Zhao, S., Zikopoulos, B., Wang, F., Brown, E.N., Wilson, M.A., 2014. State-dependent architecture of thalamic reticular subnetworks. Cell 158 (4), 808–821. https://doi.org/10.1016/j.cell.2014.06.025.

Harmelech, T., Preminger, S., Wertman, E., Malach, R., 2013. The day-after effect: long term, Hebbian-like restructuring of resting-state fMRI patterns induced by a single epoch of cortical activation. J. Neurosci. 33 (22), 9488–9497. https://doi.org/10.1523/JNEUROSCI.5911-12.2013.

Henschke, J.U., Noesselt, T., Scheich, H., Budinger, E., 2015. Possible anatomical pathways for short-latency multisensory integration processes in primary sensory cortices. Brain Struct. Funct. 220 (2), 955–977. https://doi.org/10.1007/s00429-013-0694-4.

Honey, C.J., Sporns, O., Cammoun, L., Gigandet, X., Thiran, J.P., Meuli, R., Hagmann, P., 2009. Predicting human resting-state functional connectivity from structural connectivity. Proc. Natl. Acad. Sci. Unit. States Am. 106 (6), 2035–2040. https://doi.org/10.1073/pnas.0811168106.

Hughes, S., Crunelli, V., 2013. UP states rise from the depths. Nat. Neurosci. 16 (2), 115–117. https://doi.org/10.1038/nn.3313.

Hughes, S.W., Lőrincz, M.L., Parri, H.R., Crunelli, V., 2011. Infraslow (< 0.1 Hz) oscillations in thalamic relay nuclei: basic mechanisms and significance to health and disease states. Prog. Brain Res. 193, 145–162. Elsevier.

Hwang, K., Bertolero, M.A., Liu, W.B., D'Esposito, M., 2017. The human thalamus is an integrative hub for functional brain networks. J. Neurosci. 37 (23), 5594–5607. https://doi.org/10.1523/JNEUROSCI.0067-17.2017.

Ibrahim, L.A., Mesik, L., Ji, X.Y., Fang, Q., Li, H.F., Li, Y.T., Zingg, B., Zhang, L.I., Tao, H.W., 2016. Cross-modality sharpening of visual cortical processing through

Layer-1-mediated inhibition and disinhibition. Neuron 89 (5), 1031–1045. https://doi.org/10.1016/j.neuron.2016.01.027.
Kok, P., Jehee, J.F., De Lange, F.P., 2012. Less is more: expectation sharpens representations in the primary visual cortex. Neuron 75 (2), 265–270. https://doi.org/10.1016/j.neuron.2012.04.034.
Lam, Y.-W., Sherman, S.M., 2007. Different topography of the thalamoreticular inputs to first and higher order somatosensory thalamic relays revealed using photostimulation. J. Neurophysiol. 98 (5), 2903. https://doi.org/10.1152/jn.00782.2007.
Lam, Y.-W., Sherman, S.M., 2011. Functional organization of the thalamic input to the thalamic reticular nucleus. J. Neurosci. 31 (18), 6791–6799. https://doi.org/10.1523/JNEUROSCI.3073-10.
Latchoumane, C.-F., Ngo, H.-V., Born, J., Shin, H.-S., 2017. Thalamic spindles promote memory formation during sleep through triple phase-locking of cortical, thalamic, and hippocampal rhythms. Neuron 95 (2), 424–435. https://doi.org/10.1016/j.neuron.2017.06.025.
Leong, A.T., Chan, R.W., Gao, P.P., Chan, Y.-S., Tsia, K.K., Yung, W.-H., Wu, E.X., 2016. Long-range projections coordinate distributed brain-wide neural activity with a specific spatiotemporal profile. Proc. Natl. Acad. Sci. Unit. States Am. 113 (51), E8306–E8315. https://doi.org/10.1073/pnas.1616361113.
Lewis, L.D., Voigts, J., Flores, F.J., Schmitt, L.I., Wilson, M.A., Halassa, M.M., Brown, E.N., 2015. Thalamic reticular nucleus induces fast and local modulation of arousal state. Elife 4, e08760. https://doi.org/10.7554/eLife.08760.
Li, J., Martin, S., Tricklebank, M.D., Schwarz, A.J., Gilmour, G., 2015. Task-induced modulation of intrinsic functional connectivity networks in the behaving rat. J. Neurosci. 35 (2), 658–665. https://doi.org/10.1523/JNEUROSCI.3488-14.2015.
Li, J.M., Bentley, W.J., Snyder, L.H., 2015. Functional connectivity arises from a slow rhythmic mechanism. Proc. Natl. Acad. Sci. Unit. States Am. 112 (19), E2527–E2535. https://doi.org/10.1073/pnas.1419837112.
Liang, F., Xiong, X.R., Zingg, B., Ji, X.Y., Zhang, L.I., Tao, H.W., 2015. Sensory cortical control of a visually induced arrest behavior via corticotectal projections. Neuron 86 (3), 755–767. https://doi.org/10.1016/j.neuron.2015.03.048.
Liang, M., Mouraux, A., Hu, L., Iannetti, G.D., 2013. Primary sensory cortices contain distinguishable spatial patterns of activity for each sense. Nat. Commun. 4, 1979. https://doi.org/10.1038/ncomms2979.
Liang, X., Hsu, L.M., Lu, H., Sumiyoshi, A., He, Y., Yang, Y., 2018. The rich-club organization in rat functional brain network to balance between communication cost and efficiency. Cerebr. Cortex 28 (3), 924–935. https://doi.org/10.1093/cercor/bhw416.
Liu, X., de Zwart, J.A., Scholvinck, M.L., Chang, C., Ye, F.Q., Leopold, D.A., Duyn, J.H., 2018. Subcortical evidence for a contribution of arousal to fMRI studies of brain activity. Nat. Commun. 9 (1), 395. https://doi.org/10.1038/s41467-017-02815-3.
Lorincz, M.L., Geall, F., Bao, Y., Crunelli, V., Hughes, S.W., 2009. ATP-dependent infra-slow (<0.1 Hz) oscillations in thalamic networks. PLoS One 4 (2), e4447. https://doi.org/10.1371/journal.pone.0004447.
Lorincz, M.L., Gunner, D., Bao, Y., Connelly, W.M., Isaac, J.T., Hughes, S.W., Crunelli, V., 2015. A distinct class of slow (~0.2-2 Hz) intrinsically bursting layer 5 pyramidal neurons determines UP/DOWN state dynamics in the neocortex. J. Neurosci. 35 (14), 5442–5458. https://doi.org/10.1523/JNEUROSCI.3603-14.2015.
Ma, Y., Shaik, M.A., Kozberg, M.G., Kim, S.H., Portes, J.P., Timerman, D., Hillman, E.M., 2016. Resting-state hemodynamics are spatiotemporally coupled to synchronized and symmetric neural activity in excitatory neurons. Proc. Natl. Acad. Sci. Unit. States Am. 113 (52), E8463–E8471. https://doi.org/10.1073/pnas.1525369113.
Mak-McCully, R.A., Rolland, M., Sargsyan, A., Gonzalez, C., Magnin, M., Chauvel, P., Rey, M., Bastuji, H., Halgren, E., 2017. Coordination of cortical and thalamic activity during non-REM sleep in humans. Nat. Commun. 8, 15499. https://doi.org/10.1038/ncomms15499.
Matsui, T., Murakami, T., Ohki, K., 2016. Transient neuronal coactivations embedded in globally propagating waves underlie resting-state functional connectivity. Proc. Natl. Acad. Sci. Unit. States Am. 113 (23), 6556–6561. https://doi.org/10.1073/pnas.1521299113.
McCormick, D.A., McGinley, M.J., Salkoff, D.B., 2015. Brain state dependent activity in the cortex and thalamus. Curr. Opin. Neurobiol. 31, 133–140. https://doi.org/10.1016/j.conb.2014.10.003.
Miller, K.L., Alfaro-Almagro, F., Bangerter, N.K., Thomas, D.L., Yacoub, E., Xu, J., Bartsch, A.J., Jbabdi, S., Sotiropoulos, S.N., Andersson, J.L., Griffanti, L., Douaud, G., Okell, T.W., Weale, P., Dragonu, I., Garratt, S., Hudson, S., Collins, R., Jenkinson, M., Matthews, P.M., Smith, S.M., 2016. Multimodal population brain imaging in the UK Biobank prospective epidemiological study. Nat. Neurosci. 19 (11), 1523–1536. https://doi.org/10.1038/nn.4393.
Mohajerani, M.H., Chan, A.W., Mohsenvand, M., LeDue, J., Liu, R., McVea, D.A., Boyd, J.D., Wang, Y.T., Reimers, M., Murphy, T.H., 2013. Spontaneous cortical activity alternates between motifs defined by regional axonal projections. Nat. Neurosci. 16 (10), 1426–1435. https://doi.org/10.1038/nn.3499.
Murphy, K., Fox, M.D., 2017. Towards a consensus regarding global signal regression for resting state functional connectivity MRI. Neuroimage 154, 169–173. https://doi.org/10.1016/j.neuroimage.2016.11.052.
Nair, J., Klaassen, A.L., Arato, J., Vyssotski, A.L., Harvey, M., Rainer, G., 2018. Basal forebrain contributes to default mode network regulation. Proc. Natl. Acad. Sci. Unit. States Am. 115 (6), 1352–1357. https://doi.org/10.1073/pnas.1712431115.
Nakajima, M., Halassa, M.M., 2017. Thalamic control of functional cortical connectivity. Curr. Opin. Neurobiol. 44, 127–131. https://doi.org/10.1016/j.conb.2017.04.001.
Nasrallah, F.A., To, X.V., Chen, D.Y., Routtenberg, A., Chuang, K.H., 2016. Functional connectivity MRI tracks memory networks after maze learning in rodents. Neuroimage 127, 196–202. https://doi.org/10.1016/j.neuroimage.2015.08.013.
Neske, G.T., 2015. The slow oscillation in cortical and thalamic networks: mechanisms and functions. Front. Neural Circuits 9, 88. https://doi.org/10.3389/fncir.2015.00088.
O'Reilly, J.X., Croxson, P.L., Jbabdi, S., Sallet, J., Noonan, M.P., Mars, R.B., Browning, P.G., Wilson, C.R., Mitchell, A.S., Miller, K.L., 2013. Causal effect of disconnection lesions on interhemispheric functional connectivity in rhesus monkeys. Proc. Natl. Acad. Sci. Unit. States Am. 110 (34), 13982–13987. https://doi.org/10.1073/pnas.1305062110.
Olcese, U., Bos, J.J., Vinck, M., Lankelma, J.V., van Mourik-Donga, L.B., Schlumm, F., Pennartz, C.M., 2016. Spike-based functional connectivity in cerebral cortex and hippocampus: loss of global connectivity is coupled to preservation of local connectivity during non-REM Sleep. J. Neurosci. 36 (29), 7676–7692. https://doi.org/10.1523/JNEUROSCI.4201-15.2016.
Pan, W.J., Thompson, G.J., Magnuson, M.E., Jaeger, D., Keilholz, S., 2013. Infraslow LFP correlates to resting-state fMRI BOLD signals. Neuroimage 74, 288–297. https://doi.org/10.1016/j.neuroimage.2013.02.035.
Pappalardo, L.W., Black, J.A., Waxman, S.G., 2016. Sodium channels in astroglia and microglia. Glia 64 (10), 1628–1645. https://doi.org/10.1002/glia.22967.
Park, H.J., Friston, K., 2013. Structural and functional brain networks: from connections to cognition. Science 342 (6158), 1238411. https://doi.org/10.1126/science.1238411.
Poulet, J.F., Fernandez, L.M., Crochet, S., Petersen, C.C., 2012. Thalamic control of cortical states. Nat. Neurosci. 15 (3), 370–372. https://doi.org/10.1038/nn.3035.
Power, J.D., Mitra, A., Laumann, T.O., Snyder, A.Z., Schlaggar, B.L., Petersen, S.E., 2014. Methods to detect, characterize, and remove motion artifact in resting state fMRI. Neuroimage 84, 320–341. https://doi.org/10.1016/j.neuroimage.2013.08.048.
Power, J.D., Schlaggar, B.L., Lessov-Schlaggar, C.N., Petersen, S.E., 2013. Evidence for hubs in human functional brain networks. Neuron 79 (4), 798–813. https://doi.org/10.1016/j.neuron.2013.07.035.
Quairiaux, C., Megevand, P., Kiss, J.Z., Michel, C.M., 2011. Functional development of large-scale sensorimotor cortical networks in the brain. J. Neurosci. 31 (26), 9574–9584. https://doi.org/10.1523/JNEUROSCI.5995-10.2011.
Rikhye, R.V., Wimmer, R.D., Halassa, M.M., 2018. Toward an integrative theory of thalamic function. Annu. Rev. Neurosci. 41, 163–183. https://doi.org/10.1146/annurev-neuro-080317-062144.
Roland, J.L., Snyder, A.Z., Hacker, C.D., Mitra, A., Shimony, J.S., Limbrick, D.D., Raichle, M.E., Smyth, M.D., Leuthardt, E.C., 2017. On the role of the corpus callosum in interhemispheric functional connectivity in humans. Proc. Natl. Acad. Sci. Unit. States Am. 114 (50), 13278–13283. https://doi.org/10.1073/pnas.1707050114.
Sakata, S., Harris, K.D., 2009. Laminar structure of spontaneous and sensory-evoked population activity in auditory cortex. Neuron 64 (3), 404–418. https://doi.org/10.1016/j.neuron.2009.09.020.
Schölvinck, M.L., Maier, A., Frank, Q.Y., Duyn, J.H., Leopold, D.A., 2010. Neural basis of global resting-state fMRI activity. Proc. Natl. Acad. Sci. Unit. States Am. 107 (22), 10238–10243. https://doi.org/10.1073/pnas.0913110107.
Schwalm, M., Schmid, F., Wachsmuth, L., Backhaus, H., Kronfeld, A., Aedo Jury, F., Prouvot, P.H., Fois, C., Albers, F., van Alst, T., Faber, C., Stroh, A., 2017. Cortex-wide BOLD fMRI activity reflects locally-recorded slow oscillation-associated calcium waves. Elife 6, e27602. https://doi.org/10.7554/eLife.27602.
Shen, X., Cox, S.R., Adams, M.J., Howard, D.M., Lawrie, S.M., Ritchie, S.J., Bastin, M.E., Deary, I.J., McIntosh, A.M., Whalley, H.C., 2018. Resting-state connectivity and its association with cognitive performance, educational attainment, and household income in the UK Biobank. Biol. Psychiatry: Cogn. Neurosci. Neuroimaging 3 (10), 878–886. https://doi.org/10.1016/j.bpsc.2018.06.007.
Sherman, S.M., 2016. Thalamus plays a central role in ongoing cortical functioning. Nat. Neurosci. 19 (4), 533–541. https://doi.org/10.1038/nn.4269.
Sherman, S.M., 2017. Functioning of circuits connecting thalamus and cortex. Compr. Physiol. 7 (2), 713–739. https://doi.org/10.1002/cphy.c160032.
Sheroziya, M., Timofeev, I., 2014. Global intracellular slow-wave dynamics of the thalamocortical system. J. Neurosci. 34 (26), 8875–8893. https://doi.org/10.1523/JNEUROSCI.4460-13.2014.
Sieben, K., Röder, B., Hanganu-Opatz, I.L., 2013. Oscillatory entrainment of primary somatosensory cortex encodes visual control of tactile processing. J. Neurosci. 33 (13), 5736–5749. https://doi.org/10.1523/JNEUROSCI.4432-12.2013.
Smith, S.M., Fox, P.T., Miller, K.L., Glahn, D.C., Fox, P.M., Mackay, C.E., Filippini, N., Watkins, K.E., Toro, R., Laird, A.R., Beckmann, C.F., 2009. Correspondence of the brain's functional architecture during activation and rest. Proc. Natl. Acad. Sci. Unit. States Am. 106 (31), 13040–13045. https://doi.org/10.1073/pnas.0905267106.
Smith, S.M., Vidaurre, D., Beckmann, C.F., Glasser, M.F., Jenkinson, M., Miller, K.L., Nichols, T.E., Robinson, E.C., Salimi-Khorshidi, G., Woolrich, M.W., Barch, D.M., Ugurbil, K., Van Essen, D.C., 2013. Functional connectomics from resting-state fMRI. Trends Cognit. Sci. 17 (12), 666–682. https://doi.org/10.1016/j.tics.2013.09.016.
Staresina, B.P., Bergmann, T.O., Bonnefond, M., van der Meij, R., Jensen, O., Deuker, L., Elger, C.E., Axmacher, N., Fell, J., 2015. Hierarchical nesting of slow oscillations, spindles and ripples in the human hippocampus during sleep. Nat. Neurosci. 18 (11), 1679–1686. https://doi.org/10.1038/nn.4119.
Stroh, A., Adelsberger, H., Groh, A., Ruhlmann, C., Fischer, S., Schierloh, A., Deisseroth, K., Konnerth, A., 2013. Making waves: initiation and propagation of corticothalamic Ca2+ waves in vivo. Neuron 77 (6), 1136–1150. https://doi.org/10.1016/j.neuron.2013.01.031.
Tavor, I., Parker Jones, O., Mars, R.B., Smith, S.M., Behrens, T.E., Jbabdi, S., 2016. Task-free MRI predicts individual differences in brain activity during task performance. Science 352 (6282), 216–220. https://doi.org/10.1126/science.aad8127.
Thomson, A.M., Bannister, A.P., 2003. Interlaminar connections in the neocortex. Cerebr. Cortex 13 (1), 5–14. https://doi.org/10.1093/cercor/13.1.5.

Tovar-Moll, F., Monteiro, M., Andrade, J., Bramati, I.E., Vianna-Barbosa, R., Marins, T., Rodrigues, E., Dantas, N., Behrens, T.E., de Oliveira-Souza, R., 2014. Structural and functional brain rewiring clarifies preserved interhemispheric transfer in humans born without the corpus callosum. Proc. Natl. Acad. Sci. Unit. States Am. 111 (21), 7843–7848. https://doi.org/10.1073/pnas.1400806111.

Turchi, J., Chang, C., Ye, F.Q., Russ, B.E., Yu, D.K., Cortes, C.R., Monosov, I.E., Duyn, J.H., Leopold, D.A., 2018. The basal forebrain regulates global resting-state fMRI fluctuations. Neuron 97 (4), 940–952. https://doi.org/10.1016/j.neuron.2018.01.032.

Tyszka, J.M., Kennedy, D.P., Adolphs, R., Paul, L.K., 2011. Intact bilateral resting-state networks in the absence of the corpus callosum. J. Neurosci. 31 (42), 15154–15162. https://doi.org/10.1523/JNEUROSCI.1453-11.2011.

van den Heuvel, M.P., Sporns, O., 2013. Network hubs in the human brain. Trends Cognit. Sci. 17 (12), 683–696. https://doi.org/10.1016/j.tics.2013.09.012.

Viaene, A.N., Petrof, I., Sherman, S.M., 2011a. Synaptic properties of thalamic input to layers 2/3 and 4 of primary somatosensory and auditory cortices. J. Neurophysiol. 105 (1), 279–292. https://doi.org/10.1152/jn.00747.2010.

Viaene, A.N., Petrof, I., Sherman, S.M., 2011b. Synaptic properties of thalamic input to the subgranular layers of primary somatosensory and auditory cortices in the mouse. J. Neurosci. 31 (36), 12738–12747. https://doi.org/10.1523/JNEUROSCI.1565-11.2011.

Wang, L., Saalmann, Y.B., Pinsk, M.A., Arcaro, M.J., Kastner, S., 2012. Electrophysiological low-frequency coherence and cross-frequency coupling contribute to BOLD connectivity. Neuron 76 (5), 1010–1020. https://doi.org/10.1016/j.neuron.2012.09.033.

Xiao, D., Vanni, M.P., Mitelut, C.C., Chan, A.W., LeDue, J.M., Xie, Y., Chen, A.C., Swindale, N.V., Murphy, T.H., 2017. Mapping cortical mesoscopic networks of single spiking cortical or sub-cortical neurons. Elife 6, e19976. https://doi.org/10.7554/eLife.19976.

Yan, C.-G., Cheung, B., Kelly, C., Colcombe, S., Craddock, R.C., Di Martino, A., Li, Q., Zuo, X.-N., Castellanos, F.X., Milham, M.P., 2013. A comprehensive assessment of regional variation in the impact of head micromovements on functional connectomics. Neuroimage 76, 183–201. https://doi.org/10.1016/j.neuroimage.2013.03.004.

Yan, L., Zhuo, Y., Ye, Y., Xie, S.X., An, J., Aguirre, G.K., Wang, J., 2009. Physiological origin of low-frequency drift in blood oxygen level dependent (BOLD) functional magnetic resonance imaging (fMRI). Magn. Reson. Med. 61 (4), 819–827. https://doi.org/10.1002/mrm.21902.

Yizhar, O., Fenno, L.E., Davidson, T.J., Mogri, M., Deisseroth, K., 2011. Optogenetics in neural systems. Neuron 71 (1), 9–34. https://doi.org/10.1016/j.neuron.2011.06.004.

Zalesky, A., Fornito, A., Cocchi, L., Gollo, L.L., Breakspear, M., 2014. Time-resolved resting-state brain networks. Proc. Natl. Acad. Sci. Unit. States Am. 111 (28), 10341–10346. https://doi.org/10.1073/pnas.1400181111.

Zhou, I.Y., Liang, Y.X., Chan, R.W., Gao, P.P., Cheng, J.S., Hu, Y., So, K.F., Wu, E.X., 2014. Brain resting-state functional MRI connectivity: morphological foundation and plasticity. Neuroimage 84, 1–10. https://doi.org/10.1016/j.neuroimage.2013.08.037.

Zingg, B., Hintiryan, H., Gou, L., Song, M.Y., Bay, M., Bienkowski, M.S., Foster, N.N., Yamashita, S., Bowman, I., Toga, A.W., Dong, H.W., 2014. Neural networks of the mouse neocortex. Cell 156 (5), 1096–1111. https://doi.org/10.1016/j.cell.2014.02.023.